STEM CELL BIOENERGETICS: A NOVEL REGULATORY MECHANISM FOR p107 IN ADIPOCYTE LINEAGE FATES

DEANNA PATRICIA PORRAS

A THESIS SUBMITTED TO
THE FACULTY OF GRADUATE STUDIES
IN PARTIAL FULFILLMENT OF THE REQUIREMTS
FOR THE DEGREE OF
MASTERS OF SCIENCE

GRADUATE PROGRAM IN KINESIOLOGY AND HEALTH SCIENCE

YORK UNIVERISTY

TORONTO, ONTARIO

APRIL 2015

ABSTRACT

The transcriptional co-repressor p107 has previously been shown to determine the metabolic fate of differentiated mesenchymal stem cells and their progenitors in a cell autonomous manner. Importantly, our new data shows that p107 influences stem cell fate decisions by its nuclear re-localization that results in regulating the bioenergetic status of the cells during G_0/G_1 phase of the cell cycle. In particular, p107 depleted primary stem and progenitor cells at G_0/G_1 undergo profound metabolic alterations including anaerobic glycolysis and significantly increased respiration. Our results show that p107 KD and KO stem cells and progenitors have an inefficient malate-aspartate shuttle, which decreases the availability of NADH into the mitochondria. Additionally, we found significantly elevated levels of two enzymes that enhance glycolysis, LDHa and PDK2. The effect of bioenergetics on adipocyte lineage fates is evident from inhibition of anaerobic glycolysis, which prevented the brown-type differentiation potential of p107 KD stem cell lines.

Special Acknowledgements

I would first like to thank my supervisor, Dr. Anthony Scimè. Thank you for everything you have helped me with and through. I will always remember the time I spent in your lab and all the opportunities and awesome people I have been able to meet during my time here.

I would like to thank Dr. Christopher Perry for allowing me to feel like an honorary member of his lab and for all his patients and guidance while trying to optimize my protocol in the O2K machines.

I would like to thank my continuously changing lab family, Martina, Amanda, Deb, Jerry and Maryam. Thank you for your invaluable help and support throughout these years, I am forever grateful.

Thank you to my second lab family, the 'Riddell lab' for giving me a place to discuss my excitement and at times frustration throughout this whirlwind of a journey. You guys gave me a safe haven.

Thank you to my friends and family. Especially my Mom, Dad, Grandma, Grandpa and Brother for always showing genuine interest in my research even though it always came to the conclusion that I'm going to matar ratas. Thank you for providing me with unconditional love that has helped me to conquer my first of many research dreams. I love you all and I wish you were still here Abuelito.

Most importantly, thank you to my amazing, kind, intelligent and extremely patient boyfriend Trevor. Without you I don't think I would have had the strength to finish. I love you.

TABLE OF CONTENTS

LIST OF TABLES

LIST OF FIGURES

Literature Review:

Results Section:

LIST OF ABBREVIATIONS

ATP	Adenosine triphosphate
ANOVA	Analysis of variance
Got1	Aspartate aminotransferase (cytosolic)
Got2	Aspartate aminotransferase (mitochondrial)
Bp	Base pairs
BAT	Brown adipose tissue
Brown-type	Brown and beige
Cpt1	Carnitine palmitoyltransferase 1
Cpt2	Carnitine palmitoyltransferase 2
Cat	Carnitine translocase
C/ebp	CCAAT/enhancer binding protein
Cidea	Cell Death-Inducing DFFA-Like Effector A
ChIP	Chromatin immunoprecipitation
cDNA	Complementary DNA
Cre	Cre recombinase
Cdk	Cyclin dependent kinase
Cyt c	Cytochrome c
DMSO	Dimethyl sulfoxide
DMEM	Dulbecco's modified eagle medium
ETC	Electron transport chain
Elovl3	ELOVL Fatty Acid Elongase 3
ESC	Embryonic stem cell
Fabp	Fatty acid binding protein
FAO	Fatty acid oxidation
FAS	Fatty acid synthase
Fatp	Fatty acid transport proteins
FBS	Fetal bovine serum
FADH2	Flavin adenine dinucleotide (reduced)
FACS	Fluorescent activated cell sorting
FFA	Free fatty acids
Glut	Glucose transporters
HSCs	Hematopoetic stem cells
HDAC	Histone deacetylase
HIF-1α	Hypoxia-inducible factor 1α
Idh	Isocitrate dehydrogenase
KD	Knockdown
KO	Knockout (genetically deleted)
L-carn	L-carnitine
Ldh	Lactate dehydrogenase
Mdh	Malate dehydrogenase
Mdh1	Malate dehydrogenase (cytosolic)
Mdh2	Malate dehydrogenase (mitochondrial)
MSCs	Mesenchymal stem cells
Ctl	Mesenchymal stem cells transduced with scrambled control vector

p107 KD	Mesenchymal stem cells transduced with scrambled p107 RNAi
µl	Microliters
min	Minutes
MiRO5	Mitochondrial respiration media
MEF	Murine embryonic fibroblasts
Myf5	Myogenic factor 5
NADH	Nicotinamide adenine dinucleotide (reduced)
OXPHOS	Oxidative phosphorylation
PCoA	Palmitoyl coenzyme A
PPP	Pentose phosphate pathway
Pparγ	Peroxisome proliferator activated receptor gamma
PBS	Phosphate buffered saline
Pfk2	Phosphofructokinase 2
PVDF	Polyvinylidene difluoride
PET/CT	Positron emission tomography/computed tomography
Pgc-1α	Pparγ coactivator 1 alpha
Prdm16	PRD1-BF1-RIZ1 homologous domain containing 16
Pdk	Pyruvate dehydrogenase kinase
Pdh	Pyruvate dehydrogenase
qChIP	Quantitative chromatin immunoprecipitation
qPCR	Quantitative polymerase chain reaction
Rb	Retinoblastoma susceptibility gene
pRb	Retinoblastoma susceptibility protein
RNAi	Ribonucleic acid interference
RT	Room temperature
rpm	Rotations per minute
sh	Short hair pin
SD	Standard deviation
SVF	Stromal vascular fraction
SUV39H1	Suppressor of variegation 3-9 homolog 1
TET	Ten-eleven translocation
TAGs	Triacylglycerol
TCA	Tricarboxylic acid cycle
T_3	Triiodothyronine
TBS	Tris-buffered saline
Ucp-1	Uncoupling protein 1
WAT	White adipose tissue
Wt	Wild type
ZIC1	Zic family member 1

LITERATURE REVIEW

1. Adipose Tissue

1.1 White Adipocytes

White adipocytes are morphologically unilocular in nature, storing dietary energy as triacylglycerol (TAGs) in a single lipid droplet. They are found predominately in distinct white adipose tissue (WAT) depots including intra-abdominal (visceral) and subcutaneous (Gesta et al., 2007; Cinti, 2005). During a period of caloric need, the TAGs can be rapidly hydrolyzed by lipases, a process known as lipolysis, and the resulting fatty acids are transported to other tissues to be oxidized in the mitochondria to generate energy in the form of adenosine triphosphate (ATP) (Lafontan, 2008). WAT can also function as an endocrine organ, secreting a large number of cytokines, such as leptin, interleukin-6, and tumor necrosis factor α.These cytokines are commonly referred to as adipokines, and are able to affect whole-body energy homeostasis in both normal and disease states by influencing peripheral tissues such as the liver, skeletal muscle, and the hypothalamus in the brain (Kershaw and Flier, 2004).

Under obesogenic stimuli, white adipocytes can increase in size (hypertrophy) and number (hyperplasia) leading to WAT expansion (Hirsch and Batchelor, 1976; Shepherd et al., 1993). The growth in cell number is a result of the increase in the number and subsequent differentiation of stem and progenitor cells that reside in the stromal vascular fraction (SVF) of WAT (Tang et al., 2003; Yu et al., 1997; Tang and Lane, 2012; MacDougald and Lane, 1995). Over time, the obesogenic state leads to a dramatic increase in size of individual white adipocytes causing WAT to fail as a storage vessel for lipids. Excess lipid that would normally be stored in WAT instead accumulates in various tissues such as the liver, pancreas and skeletal muscle. The overloading of free fatty acids

(FFAs) within these tissues reduces their metabolic efficiency leading to insulin resistance, β-cell dysfunction and liver steatosis (Muoio and Newgard, 2006). Additionally, increased WAT results in the dysfunctional secretion of adipokines that have adverse effects on energy use and production (Hotamisligil et al., 1994; Mohamed-Ali et al., 1997). Overall, this dysregulation causes chronic low-grade inflammation that leads to insulin resistance, dyslipidemia, type II diabetes and indirectly to cardiovascular disease (Rosen and Spiegelman, 2006).

1.2 Brown Adipocytes

In rodents, brown adipocytes that make up brown adipose tissue (BAT) are found in the interscapular, axillary, paravertebral, and perirenal regions (Park et al., 2014). More recently, Sanchez-Gurmaches and colleagues have also shown that brown adipocytes are also found residing within WAT depots of rodents (Sanchez-Gurmaches et al., 2014). Unlike white adipocytes, brown adipocytes are composed of several small lipid droplets. They are capable of synthesizing and storing TAGs but are functionally different than white adipocytes. Brown adipocytes are packed with mitochondria that contain uncoupling protein-1 (Ucp-1) in their inner membranes (Cinti, 2006). Normally, mitochondria metabolize substrates derived from glucose or fatty acids. These substrates generate reduced nicotinamide adenine dinucleotide (NADH) and reduced flavin adenine dinucleotide ($FADH_2$), which supply the electrons that pass along the electron transport chain (ETC) through the inner membrane of the mitochondria. This process forms a proton gradient in the inter membrane space and the gradient is used to drive the production of ATP through ATP Synthase (Fernie et al., 2004). However, when activated by sympathetic nerves, Ucp-1 in brown adipocytes acts as a pore, providing an alternate

pathway for protons to leak back from the intermembrane space into the matrix of the mitochondria. The result is the release of energy as heat at the expense of ATP production in a process referred to as non-shivering thermogenesis (Cannon and Nedergaard, 2004) (Figure 1). Physiologically this is tightly controlled by the sympathetic nervous system and β3-adrenergic receptors (Bachman et al., 2002; Hansen and Kristiansen, 2006; Cannon and Nedergaard, 2004). For example, when a cold stimulus is sensed the nervous system transmits the message along preganglionic neurons to postganglionic neurons that densely innervate BAT. Postganglionic neurons release the catecholamine norepinephrine, which is able to activate the adrenergic receptors on target tissues such as the β3-adrenergic receptor found on the plasma membrane of brown adipocytes (Cannon and Nederggard, 2004). Once the receptor is triggered it causes a signaling cascade to increase Ucp-1 transcription as well as activate it, which generates internal heat. Uncoupling by Ucp-1 necessitates the increased utilization of glucose and fatty acids to maintain the proton gradient to produce sufficient ATP. In order to dissipate large amounts of energy in the form of heat, brown adipocytes also express a number of other pro-thermogenic genes aside from Ucp-1, such as peroxisome proliferator-activated receptor gamma coactivator 1-alpha (Pgc-1α). Thus brown adipocytes play an important role in heat production, blood TAG clearance and glucose disposal (Cannon and Nedergaard, 2004; Bartelt et al 2011).

Brown adipocytes found in BAT are derived from the dermomyotome where skeletal muscle cells originate (Seale al., 2008). Lineage-tracing experiments using the muscle-specific myogenic factor 5 (Myf5) cre recombinase (Cre) Myf5-Cre system showed the common ancestry between skeletal muscle and brown adipocytes (Seale et

al., 2008; Lepper and Fan, 2010). In the lineage tracing experiments all cells that have ever expressed Myf5 at any time point during development are labelled by the expression of the reporter gene, green fluorescent protein. Using this system, Seale et al., showed that brown but not white fat cells arise from progenitor cells expressing Myf5, a gene previously thought to be expressed only in the myogenic lineage (Seale et al., 2008). Lepper et al. used another myogenic marker, paired box protein 7, and showed that the divergence of myoblasts and brown adipocyte progenitors occurred between embryonic days 9.5 and 11.5 in mice (Lepper and Fan, 2010). These findings helped explain why brown and not white adipocyte progenitors express myogenic genes (Timmons et al., 2007). In addition, a $Myf5^{+}$ lineage has also been attributed to a subset of brown adipocytes interspersed in WAT depots (Sanchez-Gurmaches et al., 2014).

Figure 1

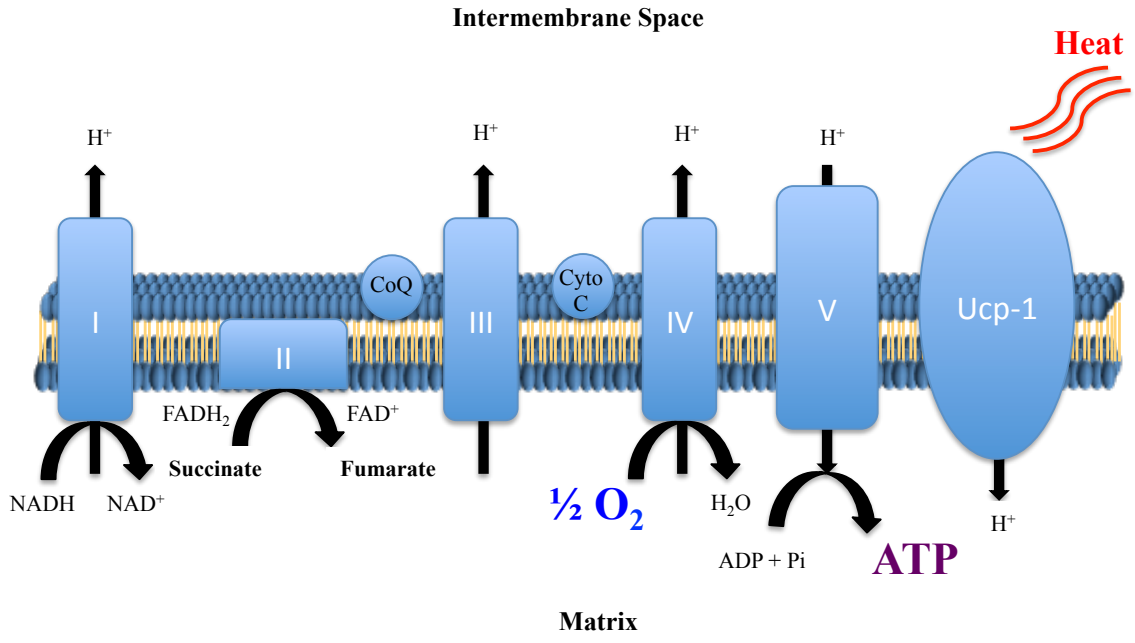

Figure 1. Diagram depicting the components of the ETC. See text for more detail.

1.3 Browning of WAT and Beige Adipocytes

Another type of fat cell is the brown like adipocyte found in WAT, known as beige or brite (brown in white) (Harms and Seale, 2013; Enerbäck, 2009; Ishibashi and Seale, 2010). The emergence of beige adipocytes within WAT occurs in response to various environmental signals such as prolonged cold exposure, adrenergic signalling and exercise (Barbatelli et al., 2010; Cinti et al., 2002; Ma et al., 2012; Boström et al., 2012; Wu et al., 2014). Beige adipocytes are very similar to brown adipocytes expressing high levels of pro-thermogenic genes including Ucp-1, and are characterized by their multilocular lipid droplet morphology, and high mitochondria content (Harms and Seale, 2013). However, other traits have been reported that differentiate brown and beige (brown-type) adipocytes in mice, including genetic variability in their occurrence, developmental origin, cell size, and elevated expression of certain transcripts (Waldén et al., 2012; Xue et al., 2007; Seale et al., 2008; Frontini and Cinti, 2010; Wu et al., 2012).

The cellular origin of beige adipocytes has not been completely elucidated. Some studies have shown a distinct progenitor population that can give rise to beige adipocytes (Lee et al., 2012; Schulz et al., 2011; Wu et al., 2012). Beige adipocytes in the epididymal WAT arise through the differentiation of progenitors that express platelet-derived growth factor receptor α, CD 34, and stem cell antigen 1 (Lee et al., 2012). Once differentiated these cells express a unique gene expression pattern different from both white and brown adipocytes (Wu et al., 2012). In 2013, Wang and colleagues used an inducible labelling system in which mature adipocytes were permanently labelled, and found that the majority of newly developed beige adipocytes were derived from *de novo* differentiation of progenitors in subcutaneous WAT (Wang et al., 2013). Alternatively,

some reports suggest that beige adipocytes are not independent cell types but result from transdifferentiation, which suggests that 'browning' and 'whitening' occurs through an interconversion of an existing mature adipocyte (Cinti, 2002; Perwitz et al., 2010; Rosenwald et al 2013). This idea emerged from the observation that cold exposure or treatment with a β3 agonist induced "browning" of retroperitoneal WAT independently of cellular proliferation (Himms-Hagen et al., 2000). Furthermore, cells with the morphological appearance of a transition state between white and brown-like have been identified (Vitali et al., 2012). Recently, Rosenwald et al. provided further evidence of transdifferentiation (Rosenwald et al., 2013). Using different genetic markers they demonstrated that beige adipocytes appear in response to an initial period of cold exposure, but subsequently take on the morphology and gene expression pattern of a typical white adipocyte after reintroduction to warm conditions. Moreover, many of these cells reactivated the thermogenic program when placed in the cold for a second time (Rosenwald et al., 2013). Taken together, *de novo* differentiation and transdifferentiation may coexist.

1.4 Characterization of Adipocyte Types in Humans

Brown adipocytes are found, in the axillary, cervical, perirenal and periadrenal regions of neonatal humans (Hu et al., 2012; Lean et al., 1986). Until recently these were thought to disappear soon after birth. However, the realization that humans possess active brown fat in adults was made with advanced positron emission tomography - computed tomography (PET/CT) technology (Cypess et al., 2009; Saito et al., 2009). PET/CT scans measuring fluorescently tagged glucose (18-fluorodeoxyglucose) uptake in cancer patients noted an increased uptake at the supraclavicular, spinal and suprarenal

regions that were not tumors but attributed to brown and/or beige adipocytes (Cypess et al., 2009; Saito et al., 2009). In 2009, Virtanen and colleagues were the first to show that the areas of cold-induced 18-fluorodeoxyglucose uptake in healthy adult subjects did in fact have the histologic features of brown fat and expressed mRNA and proteins that distinguish it from WAT (Virtanen et al., 2009).

Recently, two papers have re-examined the nature of human brown fat, helping to classify Ucp-1 positive cells as either beige or brown adipocytes. Lidell *et al*. examined the interscapular BAT depot of human neonates and found that this depot expresses Ucp-1, as well as zinc finger of the cerebellum1 (ZIC1), a selective marker for brown versus white adipocytes (Lidell et al., 2013). Importantly, ZIC1 has previously been shown to be absent in beige fat *in vitro* and *in vivo*, suggesting that neonates have only brown adipocytes (Waldén et al., 2012, Petrovic et al., 2010). However in adult humans, different fat depots of the neck revealed differences in the proportion of brown-type adipocytes that were attributed to the specific anatomical site from which they were obtained. Analysis of five different depots from the most superficial to the deepest depots (subcutaneous, subplatysmal, carotid sheath, longus colli and prevertebral) demonstrated that subcutaneous fat contained only white-like adipocyte, whereas beige-like adipocytes were located at the carotid sheath and brown adipocytes were located at the deepest site termed the musculus longus colli (Cypess et al., 2013). Interestingly, this morphological gradient was paralleled by a gradient of expression of Ucp-1 and other brown adipocyte specific genes (Cypess et al., 2013). Taken together, it appears that humans possess genuine classical brown adipocytes as neonates but as we progress into adults these regress somewhat and beige cells develop.

2. Metabolic benefits and Therapeutic Potential of Thermogenic Adipocytes

An emerging idea is that promoting the development of more brown-type adipocytes could act as a 'metabolic sink' for glucose and TAGs, and lead to an improvement in systemic glucose and lipid homeostasis.

From rodent studies, brown-type adipocytes are well established as being a powerful metabolic tissue with an immense capacity for blood TAG clearance and glucose disposal (Bartelt et al., 2011; Cannon and Nedergaard, 2004; Jakus et al., 2008). An early study surmised that it would take only 50 grams of activated BAT to sufficiently utilize 20% of an individual's daily energy needs, thus revealing the potential of BAT to help combat obesity and its associated diseases (Rothwell and Stock, 1983). Moreover, using tracer molecules for both glucose and TAG, Bartelt et al. in 2011 demonstrated that in response to an oral glucose and fat load, BAT is capable of clearing 75% and 50% of the total glucose and triglycerides from circulation, respectively (Bartelt et al., 2011). Additionally, rodents with increased amounts of brown and/or beige adipocytes are leaner and more resistant to obesity and its complications (Bartelt et al., 2011; Cousin et al., 1992; Dali-Youcef et al., 2007; Fitzgibbons et al., 2011; Scimè et al., 2005, 2010; Seale et al., 2007; Sellayah et al., 2011; Tseng et al., 2008). Alternatively, rodents with genetically deleted (KO) Ucp-1 exhibit impaired diet-induced thermogenesis (elevated metabolic rate following food ingestion) and are susceptible to becoming obese (Feldmann et al., 2009; Hamann et al., 1995, 1996; Lowell et al., 1993). Moreover, inhibition of beige adipocyte formation also promotes obesity in animals placed on a high-fat diet (Cohen et al., 2014).

Importantly, in humans, the amount of brown-type fat correlates inversely with body mass index and percentage of body fat and directly with energy expenditure during rest (van Marken Lichtenbelt et al., 2009; Cypess et al., 2009). This suggests that natural variations in brown-type adipocyte function may contribute to fluctuations in energy metabolism and thus influence body weight in humans. Brown-type adipocyte activity has also been predicted to account for 2.7% to 5% of basal metabolic rate in humans, which could cumulatively promote more than 4 kg of WAT loss during the course of one year (Frühbeck et al., 2009; Virtanen et al., 2009).

The benefits extend beyond weight loss, as investigations have revealed an inverse association of type II diabetes and activated brown fat (Ouellet et al., 2012; Lee, 2010). This is because brown-type adipocytes are very insulin sensitive, on par with skeletal muscle for glucose uptake (Orava et al., 2011). Recently, two independent research groups showed that recipient mice transplanted with human or mouse brown adipocytes, have increased lipid and glucose tolerance, enhanced insulin sensitivity, lower body weight, decreased fat mass and a complete reversal of insulin resistance when placed on a high fat diet (Nishio et al., 2012; Stanford et al., 2013). In humans, Matsushita and colleagues assessed various blood parameters using standard methods and reported that blood sugar levels, total cholesterol, and low-density lipoprotein cholesterol levels were significantly lower in cold activated BAT-positive patients versus patients without detectable BAT (Matsushita et al., 2014). Notably, using a hyperinsulinemic-euglycemic clamp, men with significant amounts of activated BAT showed an increase in whole-body glucose disposal, plasma glucose oxidation and insulin sensitivity when exposed to prolonged mild cold temperatures (Chondronikola etl al. 2014). These results

support a physiologically significant role of brown-type adipocytes in glucose homeostasis and insulin sensitivity and thus hold promise in providing a therapeutic benefit for humans.

3. Adipocyte Differentiation

In general, adipocyte formation (adipogenesis) is divided into two stages; stem cell commitment, followed by the terminal differentiation process (Lefterova et al., 2009; Tang and Lane, 2012; MacDougald and Lane, 1995). In the first step, stem cells or their progenitor cells are committed to a white, brown or beige adipocyte lineage. In the second stage, transcriptional activation of adipocyte specific genes occurs creating a specialized cell type. *In vivo*, stem cells and their progenitors receive external cues to differentiate in a quiescent (G_0) or G_1 phase of the cell cycle. In order to induce lineage commitment and adipogenesis *in vitro*, the stem cells mimic an *in vivo* state whereby they are required to be contact inhibited and in a non proliferating G_0/G_1 state (Valcourt et al., 2012).

Mesenchymal stem cells (MSCs) derived from the embryonic mesoderm are a class of stem cells with the capacity to differentiate into adipocytes (Covas et al., 2008; Lin et al., 2010). They are a part of a heterogeneous population of cells that make up the SVF of adipose tissue (Otto and Lane, 2005). They have a strong capacity for self-renewal and may differentiate into various mesodermal cell types (Abumaree et al., 2012; Elabd et al., 2007, 2009; Liu et al., 2009; Rodriguez et al., 2005). However, much of our current understanding of adipogenesis is based on studies using cell lines that are lineage committed, such as 3T3-L1. Very little is known regarding the transcriptional signals that are involved during the commitment of MSCs to the white, brown or beige lineages. In

tissue culture, the non-committed C3H10T1/2 stem cell line provides a better model to study the process of adipocyte commitment and differentiation (Bowers et al., 2006; Tang et al., 2004; Tang and Lane, 2012; Tseng et al., 2008).

Adipocyte differentiation in either white or brown fat is under the control of two key transcription factors, peroxisome proliferator-activated receptor γ (Pparγ) and the CCAAT/enhancer binding protein (C/ebp) family of transcription factors (Rosen and MacDougald, 2006). When these factors activate gene transcription they initiate a cascade of events leading to the development of a terminally differentiated adipocyte. Notably, in MSCs and C3H10T1/2 cells, the expression of both Pparγ and C/ebp induces only a white, not brown differentiation program (Rosen et al., 2000; Ahfeldt et al., 2012).

3.1 Prdm16 a molecular switch promoting the differentiation of brown fat

It is well known that the expression of the co-regulator PRD1-BF-1-RIZ1 homologous domain-containing protein 16 (Prdm16) is sufficient to drive the differentiation of stem cells and their uncommitted progenitors to the brown-type adipocyte cell fate (Kajimura et al., 2009, 2010; Seale et al., 2007, 2008). Overexpression of Prdm16 from both WAT or BAT derived SVF results in an increase in mitochondrial biogenesis, increased cellular respiration, and expression of brown-type adipocyte specific pro-thermogenic genes including Ucp-1, Pgc-1α, cell death-inducing DFFA-like effector a (Cidea) and ELOVL Fatty Acid Elongase 3 (Elovl3) (Seale et al., 2007, 2011). Notably, Prdm16 levels are higher in the more metabolically beneficial subcutaneous WAT depots containing more beige adipocytes compared to visceral depots (Kajimura et al., 2009; Seale et al., 2011). Intriguingly, a recent paper demonstrated that adipocyte-specific deletion of Prdm16 in subcutaneous fat inhibits beige adipocyte function and

formation following cold exposure or β3 agonist treatment (Cohen et al., 2014). Subcutaneous depots from the Prdm16 mutant animals acquired negative properties of visceral fat, including decreased thermogenic and increased inflammatory gene expression when placed on a high-fat diet (Cohen et al., 2014). To date, at least one paper has shown Prdm16 master regulatory role in humans. Ahfeldt and co-authors showed that white adipose cells could be differentiated from MSCs and human adipose-derived SVF cells using Pparγ2. However, when combined with both C/ebpβ and Prdm16 these cells obtained a brown fat phenotype with abundant Ucp-1 expression (Ahfeldt et al., 2012).

4. p107 and Adipogenesis

p107 (Rbl1) is part of the retinoblastoma susceptibility gene (Rb) family that also includes the protein products Rb1 (pRb) and pRbl2 (p130). pRb was first identified as the tumor suppressor gene mutated in retinoblastoma, a rare childhood cancer (Lee et al., 1987; Manning and Dyson, 2011). Subsequent research demonstrated that inactivation of pRb either directly by mutations, or indirectly through altered expression/activity of the protein's pathway lead to a variety of human cancers (Burkhard and Sage, 2008). Conversely, p107 and p130 are rarely mutated or directly inactivated in human cancers, but have altered upstream regulation in response to Rb mutations (Burkhard and Sage, 2008). The three Rb proteins are structurally similar, specifically in the pocket region, which is composed of two subdomains named A and B, separated by a 'spacer' region that is highly conserved among each of the proteins (Lee et al., 1987). Additionally, p107 and p130 also contain a cyclin dependent kinase (cdk) inhibitor domain in the N-terminus that is not present in Rb (Ewen et al., 1991; Hannon et al., 1993; Li et al., 1993; Wirt and Sage, 2010).

p107 and its family members act as co transcriptional repressors unable to bind DNA directly but can interact with members of the E2F transcription factor family. Specifically, p107 interacts with E2F4 to repress the expression of genes that are predominately involved in the cell-cycle (Muller et al., 2001; Young et al., 2003; Attwoll et al., 2004). Upon hyperphosphorylation by Cyclin/Cdk complexes, p107 becomes inactivated such that binding to E2F4 is abrogated and gene transcription is de-repressed.

The co transcriptional repression ability of this family of proteins is due to their association with a wide variety chromatin remodelling enzymes (Macaluso et al., 2006). p107 has been shown to repress E2F-dependent transcription by recruiting type 1 and 2 histone deacetylases (HDACs) and the histone methyltransferase suppressor of variegation 3-9 homolog 1 (SUV39H1) (Nicolas et al., 2003; Frolov and Dyson, 2004). Quantitative chromatin immunoprecipitation (qChIP) analyses demonstrated that p107 recruit type 1 HDACs, resulting in removal of acetyl groups from histones H3 and H4, in a compacted structure of chromatin, which prevents transcription initiation (Ferreria et al., 2001; Rayman et al., 2002).

p107, is highly regulated during adipocyte differentiation of the committed preadipocyte cell line 3T3-L1 by increasing dramatically after day 1 and disappearing by day 7 (Richon et al., 1997; Timchenko et al., 1999). The importance of p107 to adipogenesis is highlighted by the inhibition of adipocyte differentiation during its knockdown (KD) in 3T3-L1 cells (May et al., 2001). However, p107 KO murine embryonic fibroblasts (MEFs) can readily undergo adipocyte differentiation, with an increased potential over controls (Classon et al., 2000; Landsberg 2003). The findings of Scimè et al. suggested that p107 regulates stem cell commitment to determine adipocyte

lineage fate (Scimè et al., 2005). They found that p107 KO mice have a lean phenotype and display a pronounced level of beige and /or brown adipocytes with significant up regulation of Ucp-1 in WAT depots. Furthermore, these mice are resistant to weight gain when placed on a high fat diet and exhibited greater insulin tolerance than their wild type (Wt) littermate controls (Scimè et al., 2010). In 2014, De Sousa et al., revealed that suppression of p107 expression is necessary for the commitment of stem cells and their progenitors to the brown-type adipocyte lineage, providing a basis for the phenotypic character of p107 KO mice (De Sousa 2014, Scimè et al., 2005, 2010). Indeed, Prdm16 was shown to down regulate both p107 protein and mRNA levels, suggesting that p107 is a downstream target of Prdm16 in the brown-type adipocyte lineage commitment pathway.

5. Bioenergetics in Stem Cell Fate Decisions

Adult stem cells are characterized by two essential functions: their self-renewal ability and their differentiation potential, which enable them to sustain the different tissues in the body throughout the lifespan of an organism (Eckfeldt et al., 2005). Much of the research on the mechanisms governing various stem cell fates (i.e. quiescence, self-renewal or differentiation) has focused on how specific growth factors and extracellular matrix signals can elicit responses in stem cells. Interestingly, in recent years, there has been an emerging realization that, bioenergetics, which is the manner by which metabolic nutrient shuttling produces and utilizes energy, may also provide important signals that regulate stem cell properties (Figure 1). However, the biological significance and molecular mechanism underlying the metabolic regulation of stem cell fates remains largely elusive.

Figure 2

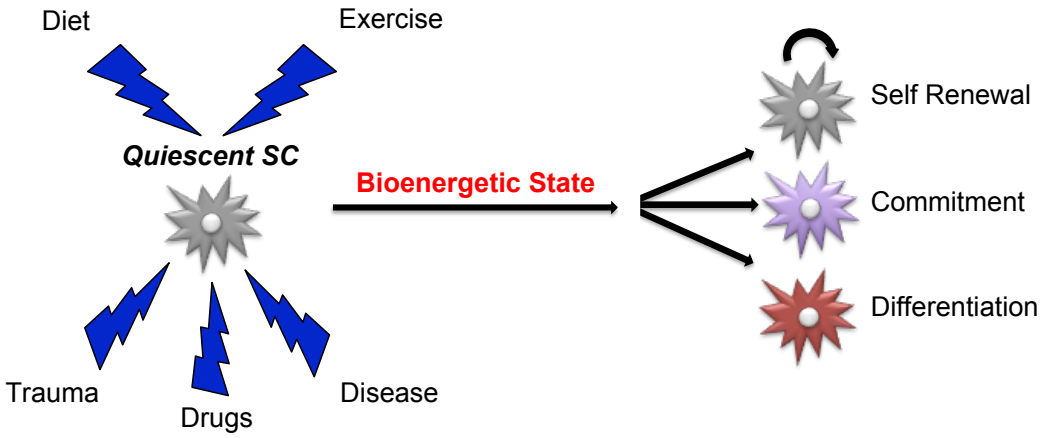

Figure 2. External cues define the metabolic character for how a stem cell will behave when activated. See text for more details.

5.1 Aerobic Glycolysis

In Mammalian cells, glycolysis is the metabolic pathway in which glucose is consumed and converted into pyruvate. Cells take up glucose through glucose transporters (Glut) where it is then metabolized to pyruvate through a series of ten enzymatic reactions. Pyruvate is then transported into the mitochondria as acetyl-CoA, through the action of pyruvate dehydrogenase (PDH), or as oxaloacetate, via pyruvate carboxylase where it is oxidized. The free energy released in the process of generating pyruvate is used to generate ATP and NADH, which can enter the mitochondria to be oxidized by the ETC.

5.2 The Tricarboxylic Acid Cycle and Oxidative Phosphorylation

The tricarboxylic acid (TCA) cycle, takes place inside the mitochondria where more NADH as well as $FADH_2$ are produced, as well as vital carbon containing intermediates, such as oxaloacetate, acetyl-CoA and α-ketoglutarate. The NADH and $FADH_2$ that are produced in the TCA cycle are oxidized through oxidative

phosphorylation (OXPHOS) by the mitochondrial ETC. The ETC is located in the mitochondrial inner membrane and result in a final reduction of molecular oxygen to water. The ETC is made up of 5 distinct complexes; complex I NADH dehydrogenase, Complex II succinate dehydrogenase, Complex III coenzyme Q-cytochrome c (Cyt c) reductase, Complex IV cytochrome oxidase and Complex V ATP synthase. Through a series of redox reactions, electrons pass along the ETC causing protons (H+) to be pumped from the matrix to the intermembrane space, creating a proton-motive force, whose energy is used by ATP synthase for the phosphorylation of ADP, generating ATP (Fernie et al., 2004).

5.3 Anaerobic Glycolysis

In the absence of oxygen, ATP cannot be formed via the mitochondria and thus pyruvate is alternatively converted into lactate, by lactate dehydrogenase (Ldh) (Figure 3). Normally, cytosolic NADH can enter the mitochondria via metabolic shuttles. However, under anaerobic conditions, where the ETC is not functioning, cytosolic NADH is oxidized in the reaction of pyruvate to lactate. Importantly, glycolysis would cease to proceed by the decrease in the NAD^+/NADH ratio if pyruvate was not converted into lactate, as its conversion provides the NAD^+ required in the pathway. Under these anaerobic conditions, glycolysis releases a small amount of useable energy that can help sustain a cell even in a state of oxygen debt. Although glycolysis is inherently less efficient, producing a fraction of ATP compared to oxidative consumption of glucose, glycolysis does enable a fast rate of energy generation in response to acute changes in energy demand (Pfeiffer et al 2001). Additionally, under abundant supply of glucose, the percentage of ATP generated from glycolysis can surpass that produced by oxygen-

dependent respiration (Guppy et al., 1993). As such, mitochondria may redirect away from oxidative ATP production thereby enabling the generation of carbon-containing intermediates, such as oxaloacetate, acetyl-CoA and α-ketoglutarate from the TCA cycle for biosynthetic purposes. In addition, generate the necessary glycolytic intermediates for the biosynthesis of new macromolecules via the pentose phosphate pathway (PPP) (Folmes et al., 2012).

Figure 3

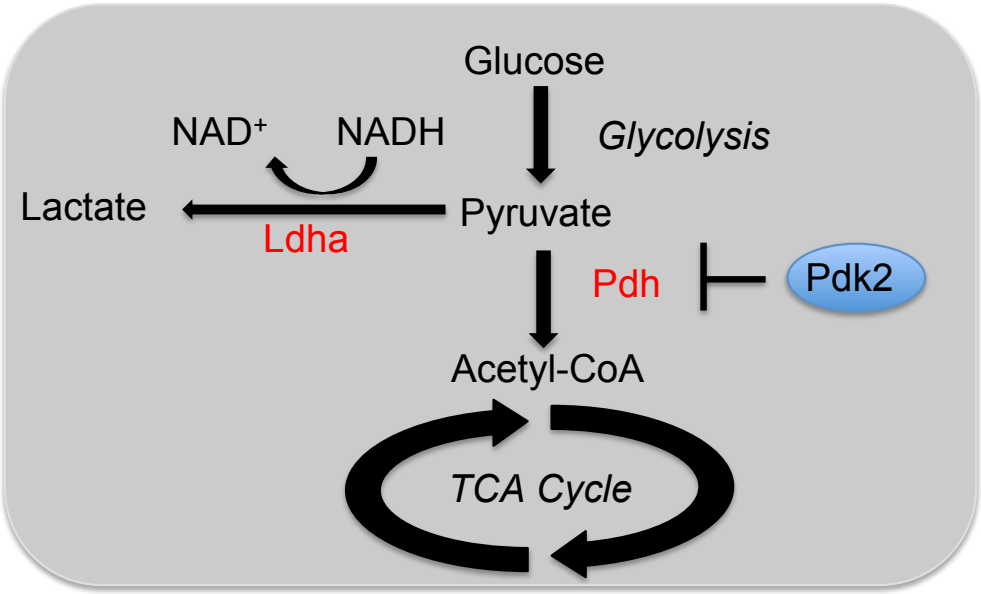

Figure 3. Diagram representing key enzymes in anaerobic glycolysis. See text for more details

5.4 NADH Mitochondrial partitioning

NADH produced from glycolysis can subsequently be oxidized by the ETC chain and generate ATP, but it cannot enter the mitochondrion directly. The primary mode of transportation of NADH into the mitochondria is the malate-aspartate shuttle system (Figure 4). The primary enzyme in the malate-aspartate shuttle is malate dehydrogenase (Mdh). Mdh is present in two forms, cytosolic malate dehydrogenase (Mdh1) and

mitochondrial malate dehydrogenase (Mdh2). In the first reaction, Mdh1 catalyses the reaction of oxaloacetate and NADH to produce malate and NAD^+. Malate is then imported from the cytosol into the mitochondrial matrix via the malate-α-ketoglutarate antiporter, which simultaneously exports α-ketoglutarate from the matrix into the cytosol. After malate reaches the mitochondrial matrix, it is converted into oxaloacetate by Mdh2, during which NAD^+ is reduced to form NADH. Oxaloacetate, which cannot be transported into the cytosol, undergoes transamination by mitochondrial aspartate aminotransferase (Got2) with glutamate to make aspartate and α -ketoglutarate. Aspartate is returned to the cytosol by the second antiporter (the glutamate-aspartate antiporter), which imports glutamate from the cytosol as it exports aspartate from the matrix to the cytosol. Once in the cytosol, aspartate is converted back to oxaloacetate by cytosolic (Got1).

Figure 4

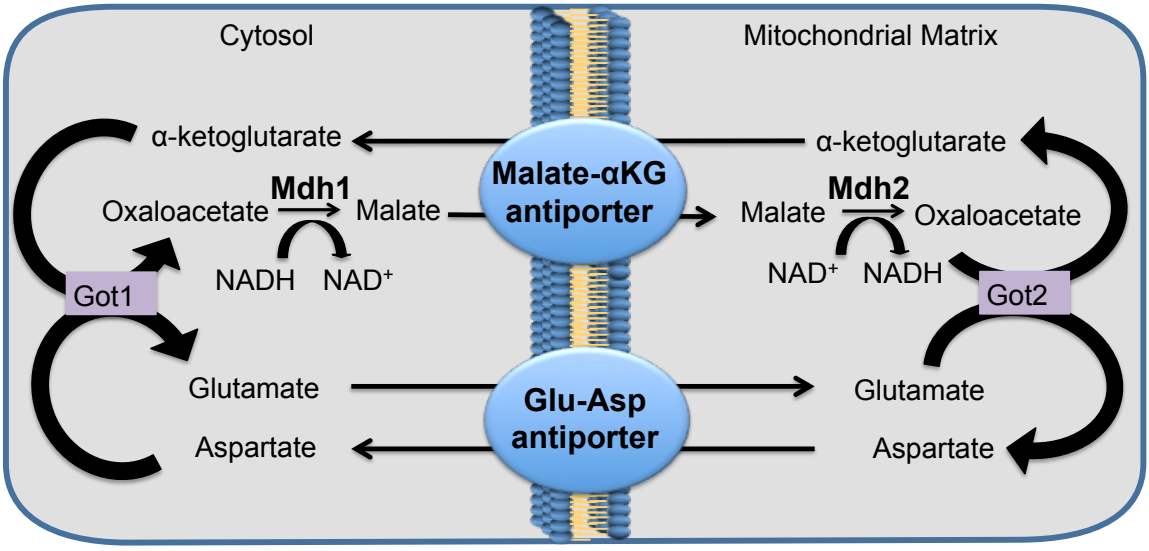

Figure 4. Diagram representing the malate-aspartate shuttle. See text for more detail.

5.5 β-oxidation of Fatty Acids

Fatty acids primarily enter a cell via fatty acid protein transporters located on the cell surface (Lopaschuk et al., 2010). The membrane associated fatty acid transporters include fatty acid translocase, tissue specific fatty acid transport proteins (Fatp), and plasma membrane bound fatty acid binding protein (Fabp) (Su and Abumrad, 2009). The oxidation of fatty acids occurs primarily within the mitochondrion and produces energy through OXPHOS. Short-chain fatty acids can pass directly into the mitochondrial matrix and form acyl-CoA derivatives and can subsequently enter β-oxidation (Berg, 2007 6th Editon). Conversely, long-chain fatty acids and their CoA derivatives are incapable of crossing the inner mitochondrial membrane (but can cross the permeable outer membrane), so a membrane transport system is necessary. Once inside the cell, a CoA group is added to the long-chain fatty acid by fatty acid synthase (FAS), forming long chain acyl-CoA. The activated fatty acid is then joined covalently to carnitine at the cytoplasmic side of the mitochondrial membrane by the transferase enzyme carnitine palmitoyltransferase 1 (Cpt1) forming fatty acylcarnitine. The conversion to acylcarnitine allows the fatty acid to be transported across the inner mitochondrial membrane via carnitine translocase (Cat), which exchanges long chain acylcarnitines for carnitine. A second transferase, carnitine palmitoyltransferase 2 (Cpt2), located on the inner mitochondrial membrane then converts the long chain acylcarnitine back to long chain acyl-CoA. The long chain acyl-CoA, now located within the mitochondrial matrix, is free to enter fatty acid β-oxidation (McGarry and Brown, 1997) (Figure 5).

Fatty acid β-oxidation is a multi-step process by which fatty acids are broken down by in the mitochondrial matrix of a cell to produce energy. In short, this cyclic

degradative pathway allows acetyl-CoA to be cleaved from a long chain acyl-CoA molecule. The number of acetyl-CoA produced depends upon the carbon length of the fatty acid being oxidized. Additionally, during β oxidation NADH and FADH2 are formed (Vance and Vance, 2008).

Figure 5

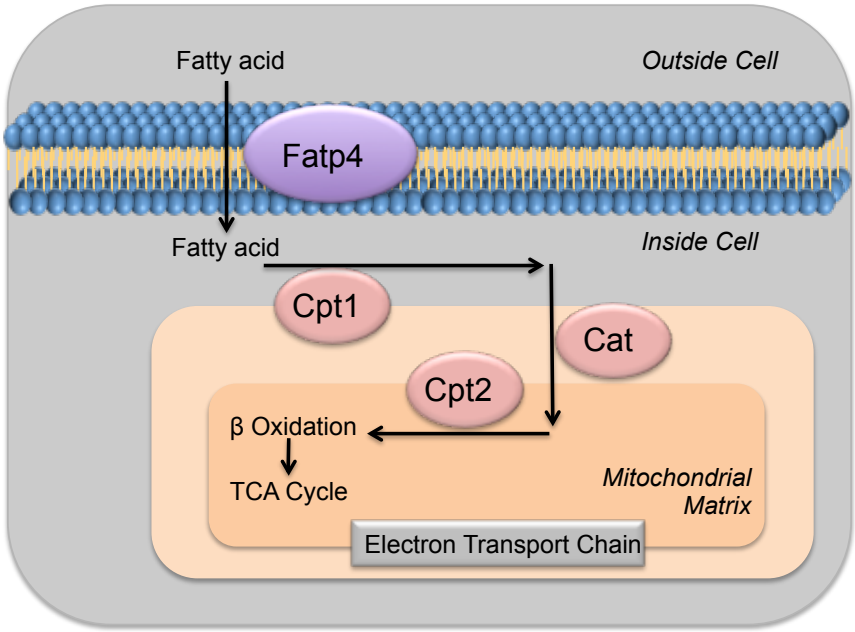

Figure 5. Diagram representing fatty acid transport into the mitochondria. See text for further details.

6. Metabolic Regulation of Stem Cell Fates

It is well known that different cell states require specific metabolic programs to support the unique demands underlying their specialized functions. Once thought to be a mere consequence of the state of a cell, it is now thought that metabolism plays an active role in dictating stem cell fates whether it be for remaining quiescent, proliferating or, differentiating (Ochocki and Simon, 2013).

6.1 Glycolysis and stem cell fates

The notion that metabolic reprogramming might play role during stem cell fate decisions originated from cellular metabolism as an underling cause of the ability of cancer cells to proliferate uncontrollably. In particular, the generation of ATP through glycolysis, despite the presence of oxygen, a phenomenon known as the Warburg effect (Lunt and Vander Heiden, 2011). The most prevalent explanation for the Warburg effect in tumors suggests that it is a strategy to deal with the anabolic demands of proliferation since many of the metabolites for energy-producing pathways are rerouted to biosynthetic pathways to support macromolecular synthesis needed in cell division (Vander Heiden, 2009; Lunt and Vander Heiden, 2011). Recent results suggest that there might be additional functions of glycolysis in the regulation of stem cell fate. For example, the induction of pluripotency is accompanied by the distinct changes in bioenergetics characterized by the conversion from an oxidative state in somatic cells to a glycolytic state in pluripotency (Folmes et al., 2011b; Zue et al., 2010; Yanes et al., 2011). Several adult stem cells also heavily rely on anaerobic glycolysis to maintain a quiescent state, and are more sensitive to oxidative stress. In hypoxic conditions, such as those found in the stem cell niche of hematopoetic stem cells (HSCs) and MSCs, the transcription factor hypoxia-inducible factor 1α (HIF-1α) promotes glycolysis as it induces the expression of pyruvate dehydrogenase kinases (PDKs) thus blocking mitochondrial respiration.

6.2 Mitochondria and oxidative phosphorylation in stem cell fates

Mitochondrial activation and remodeling of bioenergetics systems are essential in supporting the differentiation processes (Folmes et al., 2011a). In general, cellular differentiation is characterized by fully developed and functional mitochondria that have

higher ATP production through better coupling of glycolysis and TCA cycle as well as increased capacity for antioxidant defense (Panopoulos et al., 2012; Folmes et al., 2011a; Armstrong et al., 2010; Prigione et al., 2011).

MSCs have the ability to reconfigure their metabolic network to accompany such fate specification; in which changes in glycolytic pathway and mitochondrial biogenesis are the most pronounced (Liu and Ma, 2014). During adipogenic differentiation of MSCs, there is an increase in mitochondrial biogenesis, respiration, mitochondrial membrane potential, and oxygen consumption, whereas reducing mitochondrial respiration by hypoxia or by inhibition of the ETC, suppresses adipogenic differentiation (Tormos et al., 2011; Zhang et al., 2013).

6.3 Alternative metabolic Pathways in stem cell fates

Other metabolic manipulations can also affect stem cell fate decisions. For example, fatty acid oxidation (FAO) plays an important role in the maintenance of HSCs and the inhibition of the FAO pathway results in differentiation of HSC progenitors (Ito et al., 2012). Inhibition of the eicosanoid pathway, which maintains high levels of unsaturated fatty acids, preserves stem cell pluripotency, while addition of saturated metabolites to embryonic stem cell (ESC) media accelerates lineage specification (Yanes et al., 2011). This suggests that metabolic changes could not only be necessary for differentiation, but may also control it by regulating signaling pathways and gene expression directly via the metabolites they produce. Recent evidence suggests that lactate has autocrine-, paracrine- and endocrine-like actions suggesting it may function as a signaling molecule termed ‘lactoromone’, rather than a glycolytic waste product (Brooks, 2009). Specifically, research has shown that lactate can control gene expression

in several cell types as well as several proteins involved in mitochondrial activity and biogenesis (Brooks, 2009; Hashimoto et al., 2007, 2008; Samuvel et al., 2009). Carrière and colleagues demonstrated that lactate increased thermogenic gene expression in murine and human white adipocytes through Pparγ-dependent signaling (Carrière et al., 2014).

7. Metabolic Control of Epigenetics

Much of the information, regarding when and where to initiate transcription, are stored in covalent modifications of DNA and its associated proteins. The pattern of various modifications along the chromatin, such as DNA cytosine methylation and hydroxymethylation, acetylation, methylation, phosphorylation, ubiquitination, and SUMOylation of the lysine and/or arginine residues of histones determines the genome accessibility to transcriptional machinery (Ward and Thompson, 2012). Metabolic pathways are increasingly recognized to facilitate epigenetic regulation of gene expression, impacting differentiation programs (Wellen and Thompson, 2012; Kaelin and McKnight, 2013).

7.1 Acetyl-CoA and Epigenetic Regulation

In eukaryotes, the mitochondrial processes of glucose-derived pyruvate oxidation, amino acid catabolism, and the oxidation of fatty acids generate acetyl-CoA (Wagner and Payne 2011). In general, during a state of nutrient excess, a proportion of the excess acetyl-CoA generated within the mitochondria is exported into the cytosol (Bauer et al., 2005). Some of this acetyl-CoA might travel to the nucleus where it is used for histone acetylation, creating a direct link between metabolism and epigenetics (Wagner and Payne, 2011; Wallace and Fan, 2010; Wellen et al*.,* 2009). In particular, histone

acetylation leads to an open euchromatin conformation that can regulates gene expression in stem cells (Roh et al., 2005; Bernstein et al., 2006; Choudhary et al., 2009; Kaelin and McKnight, 2013). Regulation of acetyl-CoA through changes in glycolysis may contribute to epigenetic control of cell fate (Cai et al., 2011; Friis et al., 2009; Wellen et al., 2009). For example, glycolysis is thought to fuel the rise in acetyl-CoA and histone acetylation required for adipocyte differentiation (Wellen et al., 2009). In this case, during adipogenesis, activation of a lipogenic program increases glucose metabolism which fuels a rise in acetyl-CoA that is necessary for increased histone acetylation. This results in the transactivation of key metabolic proteins such as Glut4, hexokinase 2, phosphofructokinase 2 (Pfk2), and Ldh (Wellen et al., 2009).

7.2 α-ketoglutarate and Epigenetic Regulation

Similarly to acetyl-CoA, α-ketoglutarate can exit the mitochondria to function as a cofactor for enzymes, including the Jumonji-family of histone demethylases, the ten-eleven translocation (TET) family of DNA hydroxylases, which convert 5-methylcytosine to 5-hydroxymethylcytosine, and prolyl hydroxylases (PHDs) that control HIF1α transcription factor stability (Xu et al., 2011; Kaelin and McKnight, 2013). Specifically, in HSCs, MSCs, and neural progenitor cells, mutations in either isoform of isocitrate dehydrogenase (Idh), which reduces the availability of α–ketoglutarate while producing 2-hydroxyglutarate (2-HG), alter DNA and histone modifications causing premature differentiation and cancer (Figueroa et al., 2010; Sasaki et al., 2012; Lu et al., 2012). Moreover, expression of mutated Idh1 and/or Idh2, or TET depletion, impairs haemtopoietic differentiation and is accompanied by increased HSC self-renewal (Figueroa et al., 2010; Cimmino et al., 2011). Additionally, fluctuations in α-

ketoglutarate can also alter gene expression by decreasing HIF1α stability. In the presence α-ketoglutarate PHDs catalyse HIF1α hydroxylation, priming the protein for degradation. Increased HIF1α activity promotes an oxidative metabolism to glycolytic switch through transcriptional activation of genes such as Glut1 Ldha and Pdk1 (Suda et al., 2011; Zhou et al., 2012).

8. RATIONALE & OBJECTIVES

8.1 Rationale

The transcriptional co-repressor p107 has been shown to determine the fate of adult stem cells and their progenitors in a cell autonomous manner. Depletion of p107 in primary myoblasts and MSCs leads to formation of oxidative tissues, such as slow skeletal muscle fibers and brown and beige adipocytes, respectively (Scimè et al., 2005, 2010 ; De Sousa et al., 2014). Currently, there is no clear mechanism for how p107 protein levels can determine the fate of the adult stem cells. Intriguingly, one emergent mechanism for stem cell fate determination involves bioenergetics, that beyond providing fuel for a cell, is capable of engaging master genetic programs during stem cell fate decisions (McKnight, 2010).

8.2 Hypothesis

We hypothesize that p107 determines the fate of stem cells and their progenitors to the white versus brown-type adipocyte lineage by controlling the bio-energetic status.

8.3 Purpose

The purpose of this thesis is to characterize the metabolic role of p107 function in adipocyte lineage commitment.

Specific Objectives

1. To determine the mechanism(s) of p107 action during stem cell commitment by:
    a. Establishing the functional activity of p107 during stem cell commitment
    b. Assessing the effect of p107 activity on specific bioenergetics pathways
    c. Testing the influence of bioenergetics on stem cell commitment

9. MATERIALS & METHODS

Mice and dissections

All animal experiments were performed according to procedures approved by the institutional Animal Care Committee of York University. All experimental procedures were performed in adult (8 to 16 week old) mice of the Balb/c genetic background, including p107 KO mice (LeCouter et al., 1998). Mice were maintained on a standard rodent chow diet with 12-hour light and dark cycles.

Adipose depots for analysis were dissected as follows: Inguinal WAT, bilateral subcutaneous WAT depots between the skin and muscle fascia just anterior and posterior to the lower segment of the hind limbs and interscapular WAT, posterior bilateral superficial WAT depots between the skin and muscle fascia flanking either side of the BAT depot.

Cell types used

C3H10T1/2 cells are an MSC line obtained from the American Type Culture Collection. Flag tagged Prdm16 (Prdm16-Flag) and control (MSC-Ctl) cell lines were from De Sousa et al. (De Sousa et al., 2014).

MEFs, representing an enriched source of primary mesodermal stem cells, were isolated from embryos of a heterozygous p107 KO mating pair at 14.5 days post coitum. Embryos were dissected and the placenta removed. Ectodermal and endodermal cells located within heads, tails, and internal organs were discarded and some tissue saved for genotyping. The remaining mesodermal tissue was minced in 5mL of trypsin, resuspended in Dulbecco's modified eagle medium (DMEM) with 10% fetal bovine serum (FBS) and 1% penicillin/streptomycin, plated and allowed to grow.

Isolation of the SVF was performed by dissecting specific adipose depots as described above, minced and digested with 1mg/ml collagenase I (Sigma) in 10% FBS at 37°C for 45 minutes (min). To recover the cells after digestion, the cell digested slurry was passed through a 100 μm cell strainer and cells were pelleted by centrifugation at 250*g* for 5 min. C3H10T1/2 cells are an MSC line obtained from the American Type Culture Collection.

Virus production and Cell line derivation

For p107 short hairpin (sh) RNAi and control virus production, 293FT cells were transfected using Lipofectamine 2000 (Life Technologies) with p107 sh RNAi (TRCN0000218550; Sigma-Aldrich) or control scrambled p107 sh RNAi (Sigma-Aldrich) lentiviral plasmids, with packaging vectors according to manufacturer's protocol. 18 hours post transfection cells were washed and at 48 and 72 hours media containing virus was collected.

For transducing cells, 10 ml of the various collected viral media was added to C3H10T1/2 cells with 8 μg/ml of polybrene. After 24 hours cells were washed and re-fed for cell line derivation. Cell lines were selected with 2mg/ml puromycin to produce Control (Ctl) and p107 KD.

Cell culture and adipocyte differentiation

All cells were grown in DMEM supplemented with 10% FBS and 1% penicillin/streptomycin. MEFs, SVF or C3H10T1/2 cells were differentiated to adipocytes after reaching confluency to induce quiescence through contact inhibition, for 24 hours (time 0) according to the standard differentiation protocol (De Sousa et al., 2014). At time 0, DMEM with 10% FBS and 1% penicillin/streptomycin was supplemented with 0.5 mM isobutylmethylxanthine, 125 nM indomethacin, 1uM

dexamethasone, 850 nM insulin, 1nM triiodothyronine (T_3), and 1 uM rosiglitazone for 2 days. At day 2, cells were switched to maintenance medium containing 10% FBS, 1% penicillin/streptomycin, 850 nM insulin, 1 nM T_3, and 1 uM rosiglitazone for 5 days. Additionally, C3H10T1/2 cells were treated with 40mM oxamate (Sigma) or with vehicle DMSO at confluency for 24hrs and then washed and differentiated to adipocytes as described above.

Cell-cycle analysis

C3H10T1/2 cells and Wt MEFs were first washed twice with PBS, and centrifuged at 1500 rpm for 5 min at RT. The cell pellet was washed twice with ice-cold PBS and resuspended in 1mL of ice-cold PBS. This was added drop wise to 4mL of ice-cold absolute ethanol while vortexing. Cells were then fixed for 20 min at -20°C. Subsequently, the cells were pelleted by centrifuged at 1500 rpm for 5 min, and resuspended in 1mL of staining buffer (100mM Tris, pH 7.4, 150 mM NaCl, 1mM $CaCl_2$, 0.5 mM $MgCl_2$, 0.1% Nonidet P-40) containing 3μM of propidium iodine (Life Technologies) and 10ug/mL RNase A (Roche). All samples were analyzed by FACS analyses (FACSCalibur, BD Biosciences).

Protein Isolation

Cells in culture were lysed in RIPA buffer (0.5% NP-40, 0.1% sodium deoxycholate, 150 mM NaCl, 50 mM Tris-Cl pH 7.5) containing protease inhibitor cocktail (Roche) for 10 min on ice. The lysate was clarified by centrifugation at 13,000*g* for 10 min at 4°C.

Nuclear-Cytoplasmic Extraction

Monolayer cells were first washed twice with PBS, and then harvested by gentle scraping in ice-cold PBS containing protease inhibitors (Roche) and centrifuged at 1500 rpm for 5

min at RT. The supernantant was then discarded and the cell pellet was washed by suspending the cells with ice-cold PBS containing protease inhibitors (Roche) and transferred to a new 1.5 ml microcentrifuge tube and again pelleted by centrifugation at 2500*g* for 3 min. The cell pellet was then resuspended in 500uL cytoplasmic lysis buffer (10mM Tris pH 7.4, 10mM NaCl, 3mM $MgCl_2$, 0.5% NP-40 and protease inhibitors) and incubated on ice for 5 min followed by rocking at 4° for 5 min. After incubation, a small volume (150uL) of the homogenate mixture was removed. This fraction represented the "whole cell lysate". The remaining homogenate was then centrifuged at 2500*g* for 5 min at 4^{o}C. The supernatant, which represented the cytoplasmic extract, was then transferred to a clean pre-chilled tube. The cell pellet containing intact nuclei was then washed with the cytoplasmic lysis buffer. After 10 washes, the insoluble cell pellet was lysed with nuclear lysis buffer (50mM Tris pH 7.4, 5mM $MgCl_2$, 0.1 mM EDTA, 1mM dithiothreitol (DTT), 40% (wt/vol) glycerol) containing 0.15 unit/ul benzonase (Novagen) to digest the DNA and RNA in the suspension.

Western blot analysis

For Western blot analysis protein lysates were loaded onto polyacrylamide gels, ranging from 6%-15% acrylamide, and Western blotted according to standard protocol (De Sousa et al., 2014). Samples to be loaded were first boiled for 3 min in loading buffer containing 4% SDS, 10% 2-mercaptoethanol, 20% glycerol, 0.004% bromophenol blue, 0.125 M Tris-HCl, and 1mM DTT. 20µg of sample was loaded onto 7.5% SDS polyacrylamide gels or 25µg was loaded onto gradient gels (6 to 15%) for subcellular localization of p107. The proteins were separated by electrophoresis for 2 hours at 30 milliamps per gel at RT. Proteins were transferred on a 0.45 a polyvinylidene difluoride

(PVDF) membrane (Bio-Rad) at 4 °C for 120 min at 100V, using a wet transfer method. After blocking for 60 min at RT in 5% non-fat milk in Tris-buffered saline (TBS; 150mM NaCl and 50mM Tris base) containing 0.1% tween (TBST), the PVDF membranes were probed with antibodies diluted in 5% non-fat milk in TBST. Incubation with primary antibodies was performed overnight at 4 °C and with gentle rocking. Antibodies used were rabbit polyclonal C18 anti-p107 (Santa Cruz), anti- α-tubulin (Sigma-Aldrich), and anti-Histone H3 (Santa Cruz). Membranes were then washed with TBST and probed for 60 min at RT with gentle rocking with the appropriate secondary antibodies diluted in 5% non-fat milk in TBST. Secondary antibodies conjugated with horseradish peroxidase were goat anti-rabbit (Bio Rad), goat anti-mouse (Bio Rad) and rabbit anti-goat (Bio Rad) and blots were visualized with chemiluminescence on photographic film. Protein levels were then evaluated through densitometry using Image J software.

qPCR Analysis

For RNA isolation, cells were first lysed in RNA Lysis Buffer (FroggaBio) and RNA purified using the Total RNA mini kit (FroggaBio) according to the manufacturer's instructions. For RNA isolation from adipose tissue, 500 mg of isolated tissue was homogenized using the cell disruptor Retsch MM400 with two beads in 1 mL TRIzol (Invirtogen). The lysate was then centrifuged for 10 min at 13,000*g* at 4°C and the lipid layer and pellet were discarded. RNA was then extracted from the supernatant according to the manufacturer's instructions (Invirtogen). 1µg of RNA was reversed transcribed into cDNA using the GeneAmp Kit (Applied Biosystems). Reverse transcribed RNA (25ng) was used for PCR analysis. The Quantitative Real Time PCR (qPCR), assays were performed on the ABI 7500 Fast cycler (Invitrogen) and LightCycler 96 (Roche) using

SYBR green PCR Master mix (Invitrogen and Roche) with primer sets listed in Table 1. Relative expression of cDNAs was determined after normalization with β-actin using the $^{\Delta\Delta}$Ct method.

Quantitative Chromatin Immunoprecipitation Assay

qChIP assay was performed on Prdm16-Flag cells and control cell line MSC-Ctl (De Sousa et al., 2014) with an assay kit (Millipore) according to the manufacturer's instructions. Chromatin was crosslinked by formaldehyde incubation and cells were scraped in PBS containing 100 mM Na_3VO_4 and 1 mM NaF then pelleted by centrifugation followed by resuspension in SDS lysis buffer containing protease inhibitors (Roche). Crosslinked chromatin was sheared using a Bioruptor (12 cycles, 15 s shearing, 45 s at rest, 4 °C) to obtain DNA fragments to an average size 400–600 bp. One tenth of lysate was used for input and the rest was used for ChIP. Samples were pre-cleared (60 min, 4 °C) with protein A/G agarose beads (Upstate Biotechnology) then incubated with anti-E2F1 (Santa Cruz; sc-193) or M2 anti-Flag (Sigma) for 24 hrs. The immune complexes were collected by adsorption to protein A/G agarose beads (2 h, 4 °C). Beads were washed and samples eluted according to the manufacturers instructions. After purification using the Chromatin IP DNA Purification Kit (Active Motif) DNA fragments were amplified by PCR reaction. ChIP primer sets amplified the promoters of p107 (−214 to −32) forward primer cccgagctagatctccgtta and reverse primer ggcttcggggttttctttt or positive control angiotensinogen (Agt) (−127 to +23) forward primer cttggtcaagcctggattctc and reverse primer ccaacctagacaagcacagctatc. The PCR conditions were 40 cycles for 30 seconds at 95°C denaturation, 30 seconds at 56°C annealing, and 30 seconds at 72°C extension.

Measurement of mitochondrial O_2 respiration

Cells in proliferation, G_0/G_1, day 3 or day 7 of adipocyte differentiation, were first counted, resuspended in mitochondrial respiration media (MiRO5) composed of 130 mM sucrose, 60 mM K-MES, 1 mM ethylene glycol tetraacetic acid, 3 mM MgCl2, 10 mM K2HPO4, 20 mM HEPES, 1 mg/ml bovine serum albumin (pH 7.4), and permeabilized with 40 mg/ml saponin for 10 minutes at 37˚C rotation. Importantly, optimization of saponin concentration was performed by comparing the effect of a range of Saponin concentrations on State 3 respiration with exogenously added mitochondrial membrane intactness factor Cyt c for all cell types used. After permeabilization, high resolution respirometry was conducted at 37˚C with the Oxygraph-2K (Oroboros) on 10^6 cells/chamber in MiRO5 buffer. For measurement of ADP- dependent OXPHOS (State 3 respiration) the following were added sequentially: (a) 5 mM glutamate + 2 mM malate (NADH generation for complex I-supported respiration), (b) 4 mM ADP, (c) 5 mM pyruvate (complex I substrate), and (d) 5 mM succinate (FADH2 generation for complex II supported respiration). Two methods were used to assess mitochondrial O_2 consumption due to proton leak. First, measurements were made in the absence of ADP-stimulation of ATP synthase (State 2 respiration) with the addition of 5 mM glutamate and 2 mM malate to the permeabilized cells. Second, 10 mg/ml oligomycin was added, after the addition of the complex I and II components of State 3, as above. For measurement of β-oxidation the following were added sequentially: a) 2mM L-carnitine (L-carn) (fatty acid substrate) + 1 mM malate (complex I substrate), b) 100μM palmitoyl coenzyme A (PCoA).

Oil Red O Staining

After 7 days of differentiation, cells were fixed in 10% formaldehyde for 10 min at room temperature (RT), washed with water and then stained with Oil Red O solution for 20 min at RT. Oil Red O staining solution was composed of 6 volumes of stock solution containing 0.5g Oil Red O (Sigma) and 100 ml isopropanol with 4 volumes of distilled water.

Microscopy & Digital Images

Images were obtained using the Axiovert 40C Carl Zeiss microscope with ×20 0.30 LD A-Plan Ph1 Var1 objective. Digital images were captured using the Power Shot G5 camera with conversion lens adaptor LA-DC8B, 58–52 mm (Canon). Digital images of stained culture plates were captured by scanner using CanoScan LiDE 700F (Canon).

Statistical Analysis

All statistical analyses were performed on GraphPad Prism version 6.03. Student's paired t-tests were used unless otherwise stated. Results were considered to be statistically significant when $p < 0.05$. Specific data was analyzed using an appropriate one- or two-way analysis of variance (ANOVA) with a criterion of $p<0.05$. All significant differences for ANOVA testing were evaluated using a Tukey HSD post-hoc test. For these graphs, a different letter denotes a significant difference between groups. All data are mean ± standard deviation (SD).

Table 1 – List of Primers used in qPCR analysis

Primers	Forward Primer (5' – 3')	Reverse Primer (3' – 5')
Prdm16	CAGCACGGTGAAGCCATTC	GCGTGCATCCGCTTGTG
Adipoq	GCACTGGCAAGTTCTACTCAA	GTAGGTGAAGAGAACGGCCTTGT
Fabp4	ACACCGAGATTTCTTCAACTG	CCATCTAGGGTTATGATGTCTTCA
Pparγ	CAGGCTTGCTGAACGTGAAG	GGAGCACCTTGGCGAACA
Ucp1	ACTGCCACACCTCCAGTCATT	CTTTGCCTCACTCAGGATTGG
Cidea	TGCTCTTCTGTATCGCCCAGT	GCCGTGTTAAGGAATCTGCTG
Cox8b	GAACCATGAAGCCAACGACT	GCGAAGTTCACAGTGGTTCC
Elovl3	TCCGCGTTCTCATGTAGGTCT	GGACCTGATGCAACCCTATGA
Pgc-1α	CCCTGCCATTGTTAAGACC	TGCTGCTGTTCCTGTTTTC
β-actin	GCTCTGGCTCCTAGCACCAT	CCACCGATCCACACAGAGTAC
Mal-aKG antiporter	ATTGCCAGGGAAGAAGGAGT	CATGGAAGCAGCAGTGGTAA
Mdh1	CCAGAGGGAGAGTTCGTGTC	AAAGCGGTCTCCTTTTCCTC
Mdh2	AGCAGGTTCTGCCACTCTGT	AGGAGTGATCTTGCCAATGC
GOT1	TATCAGGGAGAATCGGGTTG	TAGCAATAGGGCCGAATGTC
GOT2	GTTGAAATGGGACCTCCAGA	GGGCAGGTATTCTTTGTCCA
Glu-Asp Pore	AGGCTCGCAGGTCATCTTTA	GTGAGCGTACACGGGAAAAT
LDHa	CCGTTACCTGATGGGAGAGA	GTAGGCACTGTCCACCACCT
PDK2	CTGGACCGCTTCTACCTCAG	GTTGGTGGCATTGACTTCCT
FATP4	ATTTTCGAGGGCACAGACAC	CGCCTAAGGTTGGTGTTGAT
CPT2	TCCTCGATCAAGATGGGAAC	GATCCTTCATCGGGAAGTCA
CAT	AGACTGCACCTCCTGGAAAA	ATGGCAATTTCAAAGCCAAG
CPT1b	GTCGCTTCTTCAAGGTCTGG	AAGAAAGCAGCACGTTCGAT
CPT1c	GGAAGGCAGGACAGAGACAG	CGGGACATGATGTACAGTGC

10. RESULTS

p107 KO SVF cells readily differentiate into brown-type adipocytes

Work from our lab has shown that p107 is uniquely expressed in the SVF of adipose tissue, that contains stem cells and their progenitors, but not in the terminally differentiated adipocyte fraction (De Sousa et al., 2014). Moreover, the lower expression levels of p107 are correlated with higher levels of brown-type adipocytes in adipose tissue depots (Scimè et al., 2005, 2010; De Sousa et al., 2014). We tested whether p107 expression levels control adipocyte lineage commitment in primary adult stem cells in an autonomous manner. For this, the differentiation potential of SVF cells from subcutaneous fat pads of (Wt) compared to p107 KO mice was assessed. Oil Red O staining 7 days post-differentiation revealed that adipocyte differentiation was somewhat higher for the SVF of p107 KO as compared to Wt mice (Figure 6A). Gene expression analysis of general adipogenic markers *Adipoq* and *Fabp4* showed no difference in levels, but *Ppar*γ levels were significantly increased in the differentiated SVF of p107 KO mice (Figure 6B). This increase might be reflective of the known enhanced adipocyte differentiation capacity of p107 KO SVF cells (Scimè et al., 2005). Importantly adipocytes derived from p107 KO mice had at least an eleven-fold significantly (p <0.001) higher gene expression level of the brown-type adipocyte marker *Ucp-1* (Figure 6C). Convincingly, the thermogenic character of these cells showed significantly higher expression levels of other brown-type markers, *Cidea ($p<0.0001$), Cox8b($p<0.0001$), Elovl3($p<0.01$), Pgc-1α($p<0.0001$)* and *Prdm16($p<0.0001$)* (Figure 6C). These results suggest that p107 functions in primary adult stem and/or progenitor cells to block brown-type adipocyte differentiation.

Prdm16 regulates p107 gene expression directly

We investigated the potential upstream control of p10 in brown-type adipocyte determination. The brown fat determination factor, Prdm16, down regulates both p107 protein and mRNA levels (De Sousa et al., 2014). Using a qChIP assay we assessed Prdm16-bound DNA regions on the p107 promoter. In these experiments, C3H10T1/2 cells expressing Flag tagged Prdm16 (Prdm16-Flag) or control vector (MSC-Ctl) cell lines (De Sousa et al., 2014) were immunoprecipitated and purified using anti-Flag antibodies (Figure 7A). Prdm16 specific binding was evaluated by qPCR with primer sets within the 900 base pair (bp) promoter of p107 and to the positive control promoter, angiotensinogen (Agt) (Kajimura et al., 2008). An E2F1 immunoprecipitation was used as a positive control for interaction at the p107 promoter (Figure 7B). As expected, E2F1 bound to the p107 promoter in C3H10T1/2 cells and not to the Agt promoter (Figure 7C). Importantly, Prdm16 was enriched at both the p107 and Agt promoters, but only in the cells engineered to express Flag-Prdm16 (Figure 7D). Together, these data suggest that Prdm16 directly down regulates p107 gene expression during the commitment stage of brown-type adipocyte development.

p107 is active in G_0/G_1 after nuclear translocation

We also wanted to find the downstream mechanism for how p107 functions in adipocyte lineage fates of stem cells. We first determined its potential activity during the earliest phases of differentiation, at confluency before addition of differentiation media when lineage fate choices are made. As p107 is a transcriptional co-repressor, we assessed its subcellular localization and protein levels in the stem cell line, C3H10T1/2, and primary MEFs, an enriched source of mesodermal stem cells and progenitors. By

western blotting of cytoplasmic and nuclear fractions, we found that it is almost exclusively expressed during proliferation in the cytoplasm of both MEFs and C3H10T1/2 cells (Figure 8A and 8B**).** However, as the cells become confluent, p107 translocates transiently into the nucleus becoming negligible after 24 hours and is barely existent at 48 hours (Figure 8A and 8B). The timing of p107 nuclear localization corresponds to the time point when cells are contact inhibited before the addition of adipocyte differentiation media.

We next assessed the cell cycle phases for C3H10T1/2 cells and MEFs, during the same time points that had been done for the subcellular localization experiments. Using flow cytometric analysis with propidium iodide DNA staining, we found that during proliferation, the cells are mainly in S phase (Figure 8C). Importantly, when either C3H10T/2 cells or MEFs reached confluency, they entered a non-proliferative G_0/G_1 state (Figure 8C). This is the time point when adipocyte differentiation media is added to promote efficient differentiation.

p107 influences cellular respiration

We assessed the influence of p107 on bioenergetics by first testing the oxidative capacity of p107 KO and Wt MEFs. Using high resolution respirometry of permeabilized cells during proliferation, G_0/G_1 and 3 and 7 days post adipocyte differentiation was measured using an Oroboros Oxygraph-2k. Substrates were added in a sequential order to activate various components of the ETC (Figure 9A). ADP-stimulated respiration (State 3 respiration), supported by both complex I and complex II substrates glutamate and malate, (GM), with pyruvate, (GMP) and together with succinate (GMPS), resulted in significantly greater oxygen consumption in p107 KO MEFs compared to Wt control

cells at G_0/G_1 ($p<0.001$, GM_3; $p<0.001$, GMP_3; $p<0.01$, $GMPS_3$) and 3 ($p<0.0001$, GM_3; $p<0.01$, GMP_3; $p<0.05$, $GMPS_3$), and 7 ($p<0.001$, GM_3; $p<0.05$, GMP_3; $p<0.05$, $GMPS_3$) days post differentiation (Figure 9B). Notably, during the proliferative state, there tended to be minimal differences in the oxidative capacity of p107 KO stem cells in comparison to control cells (Figure 9B). Moreover, p107 KO MEFs exhibited greater uncoupled respiration than control cells when treated with substrates for complex I (GM) or both complex I and II substrates (GMPS) with oligomycin, during each time point (Figure 9B). Taken together, this data indicates that both the oxidative and thermogenic capacities of p107 KO MEFs are significantly enhanced during differentiation as well as in G_0/G_1 before the addition of differentiation media.

In order to discriminate against any possible developmental effects caused by chronic loss of p107 in MEFs and to better maintain a homogenous population of cells, we assessed the influence of p107 on bioenergetics with p107 KD C3H10T1/2 cell lines compared to their controls. We used lentivirus to deliver a short hairpin sequence for targeting p107 mRNA (shp107) or a non-targeting scrambled control to produce cell lines designated p107 KD and control (Ctl), respectively. Western blot analysis revealed that p107 protein levels were significantly ($p< .0001$) reduced by as much as 95% with expression of shp107 in comparison to untransduced cells and Ctl (Figure 10A).

The oxygen consumption of p107 KD cells compared to their controls was assessed during proliferation, G_0/G_1 and, 3 and 7 days post differentiation, as was done for the MEFs in Figure 9. Corroborating the p107 KO MEF results, high resolution respirometry revealed that during State 3 respiration, the p107 KD cells had significantly greater oxygen consumption than control cells at G_0/G_1 ($p<0.001$, GM_3; $p<0.05$, GMP_3)

and at 3 ($p<0.001$, GM_3; $p<0.01$, GMP_3; $p<0.01$, $GMPS_3$) and 7 ($p<0.0001$, GM_3; $p<0.0001$, GMP_3; $p<0.0001$, $GMPS_3$) days post differentiation (Figure 10B). Again as with the MEFs, during the proliferative state, there were no differences in the oxidative capacity of p107 KD stem cells in comparison to control cells (Figure 10B). In addition, a greater respiration due to proton leak occurred when supported by oligomycin for each day in differentiation (Figure 10B). Together, these data confirm that the oxidative and thermogenic capacities of the p107 KO and KD stem cells during differentiation are significantly enhanced beginning at G_0/G_1 before addition of adipocyte differentiation media and during adipocyte differentiation.

p107 KO and KD stem cells have altered NADH partitioning in G_0/G_1

We tested if p107 KO and KD stem cells had a better coupling of glycolysis and TCA that might potentially account for the increased respiration in G_0/G_1. We first assessed, for p107 KO and Wt MEFs, the gene expression of components of the malate-aspartate shuttle system, which provides the essential reducing equivalents from glycolysis to the ETC (Figure 4). As anticipated, we found no significant differences in components of the shuttle during the proliferative state (Figure 11A). Surprisingly, gene expression levels of key components of the shuttle system were significantly reduced including the *Glu-Asp pore ($p<0.05$), Mal-aKG pore ($p<0.01$),* and *Mdh1 ($p<0.05$)* in p107 KO stem cells in comparison to control cells at G_0/G_1(Figure 10B). We also performed this analysis on p107 KD cells compared to control cells in G_0/G_1 and during proliferation. We found that during proliferation there were no differences in the gene expression pattern of the malate-aspartate shuttle between p107 KD and control cells, corroborating the results with MEFs (Figure 11A and Figure 11C). However, we found

significantly reduced gene expression levels of the *Glu-Asp pore (*$p<0.05$*), Mal-aKG pore (*$p<0.05$*)*, and *Mdh1 (*$p<0.01$*)* in p107 KD cells in comparison to control cells at G_0/G_1 (Figure 11D).

p107 KO and KD stem cells participate in anaerobic glycolysis at G_0/G_1

Glycolytic coupling to the TCA and ETC was further analyzed by assessing key components of pyruvate oxidation. We first assessed Ldha that promotes the conversion of pyruvate to lactate transforming NADH to NAD+, which is used in glycolysis. Gene expression analysis by qPCR showed significantly ($p<0.05$) increased *Ldha* expression in p107 KO MEFs at G_0/G_1 in comparison to Wt, and to p107 KO MEFs and Wt cells during proliferation (Figure 12A). Additionally, by Western blotting, p107 KO MEFs had significantly ($p<0.001$) increased Ldha protein levels at G_0/G_1 in comparison to Wt cells, and to both Wt and p107 KO MEFs during proliferation (Figure 12B).

Comparing p107 KD cells versus control cells during G_0/G_1 and proliferation corroborated the results for MEFs. We found significantly ($p<0.01$), increased levels of *Ldha*, gene expression by qPCR for p107 KD in G_0/G_1 compared to controls and to both p107 KD and control cells during proliferation (Figure 12C). By Western blotting, we also found significantly ($p<0.01$) increased levels of Ldha, protein for p107 KD in G_0/G_1 compared to control cells and to both p107 KD and controls during proliferation (Figure 12D).

We also tested the gene and protein expression of PDK2, which inhibits the activity of PDH responsible for transforming pyruvate into acetyl-CoA. qPCR analysis revealed that PDK2 gene expression was significantly increased ($p<0.05$) in p107 KO stem cells in comparison to Wt cells, as well as p107 KO MEFs and Wt cells during

proliferation (Figure 13A). Moreover, protein levels were also significantly increased ($p<0.001$) in p107 KO MEFs at G_0/G_1 in comparison to Wt cells (Figure 13B). Notably, this increase only occured at G_0/G_1 as there were again no significant differences in PDK2 gene and protein levels between p107 KO and Wt during a proliferative state (Figure 13B).

p107 KD cells, in comparison to control cells at G_0/G_1 and versus p107 KD cells and controls during proliferation, also showed a significant increase in both PDK2 gene ($p<0.05$) and protein levels ($p<0.01$) (Figure 13C and 13D). This verified our previous results obtained from the p107 KO MEFs. Again, there were no significant differences in PDK2 gene and protein levels between p107 KO and control cells during proliferation.

p107 KD cells have enhanced β-oxidation in G_0/G_1

We also assessed the capacity of β-oxidation that might potentially account for the increased respiration in G_0/G_1 for p107 KO and KD cells. To accomplish this, we used high resolution respirometry and stimulated β-oxidation by adding the following substrates sequentially: fatty acid substrate L-carn, malate a complex I substrate, and fatty acid substrate PCoA (Figure 14A). As anticipated, there were no significant differences between p107 KD and control cells during proliferation, but at G_0/G_1 p107 KD cells demonstrated significantly ($p<0.05$) enhanced β-oxidation (Figure 14B).

We also tested for various components of fatty acid transport and metabolism to determine if they might have contributed to the enhanced β-oxidation in p107-depleted stem cells at G_0/G_1. qPCR gene expression analysis revealed that p107 KD compared to control cell lines had increased components of fatty acid transport and metabolism in G_0/G_1 (Figure 14C). Specifically, p107 KD stem cells had a 7-fold increase in *Fatp4*

(p<0.05) and 4-fold increase of *Cpt2* (p<0.05), whereas there were no significant differences between p107 KD cell in comparison to control cells during proliferation.

Anaerobic glycolysis in G_0/G_1 is necessary for brown-type differentiation

To explore how altered bioenergetics affect adipocyte lineage fates through p107, we used the chemical oxamate that inhibits Ldha and thus glycolysis in adipocyte differentiation assays. Oil Red O staining 7 days post-differentiation of p107 KD and control cells revealed that adipocyte differentiation was unaffected by oxamate treatment (Figure 15A). In support of our published data (De Sousa et al., 2014), the p107 KD cells had a significantly higher expression level of Ucp-1 (p<0.05) 7 days post differentiation. However, inhibition of anaerobic glycolysis via oxamate administration prevented the brown-type differentiation potential of p107 KD stem cells (Figure 15B). There were no significant increases in Ucp-1 gene expression in both treated and untreated control cells (Figure 15B).

11. DISCUSSION

In this study, we provide mechanistic evidence for how the transcriptional co-repressor p107, acts as an adipocyte lineage determinant factor. The importance of p107 in adipocyte fat lineage decisions in a stem cell-autonomous manner is assured by our assessment of the differentiation capacity of primary stem and progenitor cells. For this we used the SVF of adipose depots from mice that contain the cells that might become adipocytes during its lifetime. Contrary to their Wt controls, SVF cells of p107 KO mice have the ability to differentiate into brown adipocytes, confirmed by the expression of Ucp-1 and other pro-thermogenic markers (Figure 6C). A result that corroborates the data obtained from both p107 KO MEFs and p107 KD stem cell lines (De Sousa et al., 2014). These results indicate that p107 acts as a crucial factor within a signaling cascade involved in adipose development during adulthood. This is highlighted by the down regulation of p107 gene and protein expression in the presence of the master regulator of brown-type adipocyte formation, Prdm16 (De Sousa et al., 2014). We found using qChIP assays that Prdm16 does this by directly binding the promoter region of p107 (Figure 7D).

In this study, we show for the first time that p107 controls adipocyte lineage fate decisions of white versus brown-type adipocytes by its nuclear re-localization during G_0/G_1 phase of the cell cycle. We demonstrated that both genetic and shRNA-mediated reduction of p107 in stem cells at G_0/G_1 resulted in profound metabolic alterations including anaerobic glycolysis and significantly increased respiration. Specifically, we found that p107 is almost exclusively expressed during proliferation in the cytoplasm of primary Wt MEFs and the non-committed C3H10T1/2 stem cell line (Figure 8A and 8B).

However, as both cell types become confluent and enter a G_0/G_1 state (Figure 8C), p107 translocates transiently into the nucleus becoming negligible after 24 hours (Figure 8A and 8B). As p107 is a co transcriptional repressor, its nuclear translocation corresponds to its active role during lineage commitment. It is during this G_0/G_1 stage, when a cell makes important decisions to remain quiescent, proliferate or differentiate (Loyer et al., 1996; Zavitz and Zipursky, 1997). Importantly, it is also the time point in which adipocyte differentiation is initiated (De Sousa et al., 2014; Rosen and MacDougald, 2006). Together, this suggests that p107 functions in adipocyte lineage decisions within a short window, after it is translocated to the nucleus.

During the proliferative state, there were no differences in the oxidative capacity of p107 KO MEFs and KD C3H10T1/2 cells in comparison to their controls (Figure 9B and Figure 10B). However, the difference in respiration levels became significantly increased in cells lacking p107 only when they entered the G_0/G_1 state. This suggests that during the non-proliferating state, p107 functions in lineage commitment to suppress pro thermogenic and oxidative gene expression.

It is tempting to speculate that the higher rates of oxidation might be coupled to increased availability of NADH from aerobic glycolysis. Interestingly, we found the malate-aspartate shuttle, which is necessary to transfer NADH from the cytoplasm to the mitochondria, to be deficient (Figure 11B and 11D). This inefficiency could decrease the capacity for the re-oxidation of NADH in the mitochondria, allowing it to be used by Ldha to convert pyruvate into lactate, generating NAD+ in the process, which drives glycolysis. This possibility was strongly reinforced by robust increases in both gene and protein expression levels of Ldha (Figure 12) and Pdk2 (Figure 13) in p107-depleted

stem cells at G_0/G_1. This shift in metabolism creates a Warburg-like effect in the G_0/G_1 stem cells with changes in glycolytic NADH partitioning that enhances glycolysis and decouples it from the TCA and ETC through alterations in pyruvate metabolism. However, we found that glucose oxidation might be compensated by increased fatty acid β-oxidation during G_0/G_1 and that this was correlated to an increase in fatty acid transport protein components that could allow p107-depleted stem cells to better utilize fatty acids as substrates (Figure 14).

We also demonstrated the importance of metabolic reprogramming for brown-type adipocyte differentiation by utilizing oxamate, a chemical inhibitor of glycolysis. Inhibition of Ldha and thus anaerobic glycolysis by oxamate administration at G_0/G_1 prevented the brown-type differentiation potential of p107 KD stem cells. Whereas untreated p107 KD stem cells had a significant increase in the brown-type adipocyte marker, Ucp1 (Figure 15). Together, this data provides compelling evidence for the novel role of p107 in bioenergetic remodeling of MSCs that is required to control stem cells and progenitor cells in adipocyte lineage fate decisions. Indeed, Teperino and colleagues showed a Warburg-like metabolism in brown fat (Teperino et al., 2012). Though we are currently unsure of the precise mechanism by which producing a Warburg-like metabolic state at G_0/G_1 helps in commitment, future research could make use of glycolytic chemical inhibitors to dissect different metabolic pathways. It would be interesting to see if inhibition with other key glycolytic enzymes such as dichloroacetic acid, a chemical inhibitor of Pdk2, would prevent a brown phenotype.

Translocation of p107 into the nucleus correlated to its active state when it is bound to DNA promoters repressing gene expression. We would expect p107-binding

sites on promoters of pro thermogenic genes, or genes involved in bioenergetic remodeling. To identify p107 global binding sites across the entire genome, ChIP-sequencing (ChIP-seq), which combines ChIP with global DNA sequencing to identify the genome wide binding sites of DNA-associated proteins, would need to be performed.

The profound changes in the oxidative phenotype of the differentiated adipocytes emanating from p107 depleted G_0/G_1 state suggest that p107 might be a key player in epigenetic modification for stem cell commitment. For adipocyte lineage fates, inactivating specific genes might allow the stem cell to commit to the white versus brown fat lineage. On the other hand, it is conceivable that when signals are sent during the commitment of the stem cells to become a brown-like adipocyte, p107 is down regulated in order to prevent the remodeling of the chromatin on the oxidative promoters. Indeed, early in G_1 phase of the cell cycle, p107 can complex with E2F4 and bind HDAC and remodel chromatin causing the repression of gene transcription (Kennedy et al., 2000; Macaluso et al., 2006; Zini et al., 2001; Wirt and Sage, 2010). Another important target of chromatin silencing is tri methylation of lysine 9 of histone H3 (H3K9) by the methyl transferase SUV39H1 (Martin and Zang, 2005). SUV39H1 is known to interact with p107 on promoters to target H3K9 for methylation to repress gene expression (Nicolas et al., 2003). Importantly, this would provide an explanation as to why p107 would be required to exert its effect at an early time point during the commitment of the stem cell and would be of little importance in an already terminally differentiated adipocyte, where it has been shown to no longer exist (De Sousa et al., 2014). Alternatively, different chromatin modification by p107 may be occurring. To ascertain if p107 functions by

influencing epigenetic remodeling, p107 ChIP-seq, compared to histone H3 tri methyl K9 ChIP seq, in the absence or presence of p107 would need to be done.

Recent evidence suggests that the availability of the necessary metabolites in histone and DNA modifications modulates epigenetic alterations, providing a direct link between metabolic reprogramming and gene expression. For example, high levels of acetyl-CoA can promote histone acetylation and the activation of genes (Agathocleous and Harris et al., 2013). It is not clear if p107-depleted cells have elevated levels of acetyl-CoA. p107-depleted stem cells undergo aerobic glycolysis at G_0/G_1, with significant increases of Ldha and Pdk2, such that pyruvate is converted into lactate and not acetyl–CoA by Pdh. However, acetyl-CoA can be made from the conversion of pyruvate into oxaloacetate by carboxylase that forms citrate in the mitochondria (Cheng et al., 2011). The mitochondrial citrate can then be exported to the cytosol where it is reconverted into acetyl-CoA by ACL. This is highly relevant in that the acetyl-CoA groups used to modify histones are predominantly produced by ACL enzyme (Wellen et al., 2009). Importantly, exporting citrate to the cytoplasm may stop the TCA cycle unless additional pathways are engaged to supply oxaloacetate to keep the cycle going (Zaidi et al., 2012). Hence, a compensatory mechanism in which pyruvate is carboxylated to form oxaloacetate would be required in p107-depleted stem cells to maintain TCA cycling. Nonetheless, pyruvate might still enter the mitochondria via Pdh since increased levels of Pdk2 protein have not yet been correlated to increased enzymatic activity.

Classically, p107 functions by repressing gene promoters involved in cell cycle progression (Zhu et al., 1993). Moreover, shortening of the G_1-phase of the cell cycle is caused by the down regulation of several regulators of the cell cycle including p107

(Pinto et al., 2008). Interestingly, the G_1-phase of the cell cycle provides an opportunity for cells to become influenced by intrinsic and extrinsic factors, to develop new signaling pathways, and undergo chromatin modifications (Orford et al., 2008; Lange et al; 2010). Therefore, time spent at this stage might be a critical factor for cell fate changes to occur. Vanderluit et al. in 2007 provided evidence that a shortened G1 phase due to loss of p107 regulates the transition from a progenitor cell to a committed neuroblast (Vanderluit et al., 2007). In line with this, it is reasonable to suggest that the knockdown or complete absence of p107 expression may result in a shortened G_1 phase allowing uncommitted stem cells to become brown-like adipocytes. In contrast, factors involved in white adipocyte commitment would require a greater length of time in G_1 to bring about their lineage-specific effects. Enhanced glycolytic flux has also been shown to trigger exit out of G_0/G_1 by regulating core components of the cell cycle machinery. Glucose can shorten this period by increasing the build-up of cyclin D2 (Salpeter et al., 2011). Transcriptional regulation of cyclin D2 is controlled by the carbohydrate response element binding protein (ChREP) that are regulated by several glucose-derived metabolites, including glucose-6-phosphate, and fructose 2,6 biphosphate (Metukuri et al., 2012; Diaz-Moralli et al., 2012; Arden et al., 2012). This has only be characterized in hepatocyte and the beta-cells of the pancreas. Yet, it is plausible that anaerobic glycolysis depicted in p107-depleted stem cells, may be another contributing factor in shortening G_1 phase allowing the uncommitted stem cells to become brown-like adipocytes.

12. CONCLUSION

Given its integral role in regulating systemic metabolism and energy homeostasis, it is no surprise that adipose tissue, consisting of white, brown and beige adipocytes, has become an important therapeutic target in the battle against obesity and its associated metabolic diseases. Thermogenic and highly oxidative brown and beige adipocytes have been shown to protect animals against obesity and improve glycemic control. Hence, encouraging stem cells to preferentially differentiate into this type of fat represents a promising treatment strategy. In recent years, there has been an emerging realization that, in addition to growth factors and extracellular matrix cues, metabolic pathways may also provide important signals that regulate stem cell fate decisions. Though little is known about the mechanisms that commit stem cells toward different adipocyte lineages, still less is known about metabolic regulation in adipocyte lineage determination. Once thought to be a mere consequence of the state of a cell, metabolic regulation, as evidenced by this study, plays a pivotal role in dictating adipocyte lineage fate decisions (Figure 16). Here we show for the first time that p107 controls adipocyte lineage fate decisions of white versus brown-type adipocytes by its nuclear re-localization that results in regulating the bioenergetic status of stem and progenitor cells during G_0/G_1 phase of the cell cycle. Nevertheless, the precise mechanism for how p107 functions during lineage commitment of adipocytes remains to be elucidated. Future experiments should focus on elucidating the mechanism of p107 translocation as well as its promoter targets once in the nucleus.

13. FIGURES

Figure 1

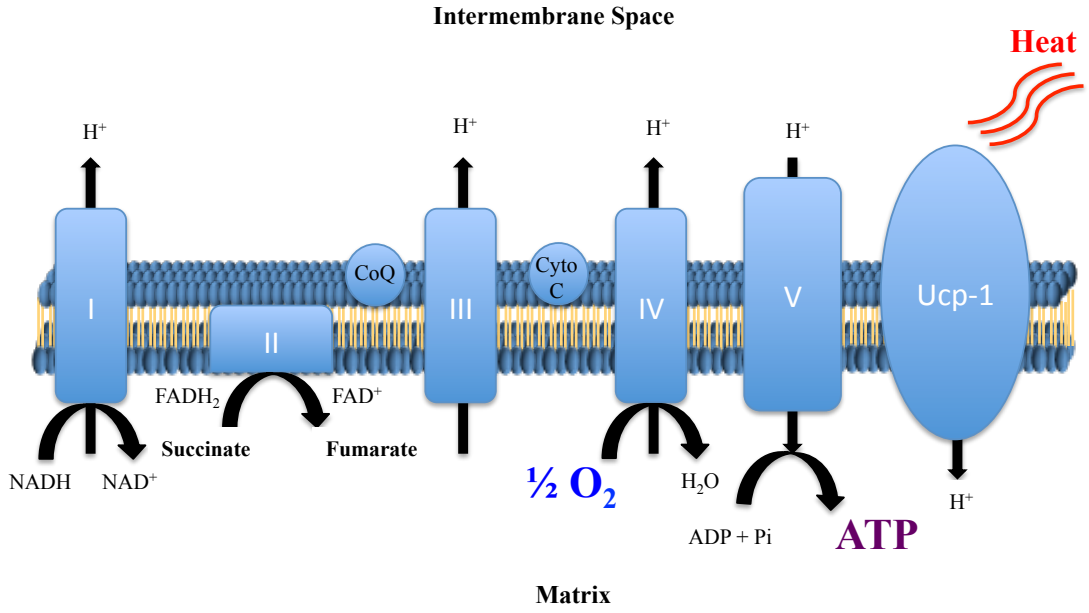

Figure 1. Diagram depicting the components of the ETC. See text for more detail.

Figure 2

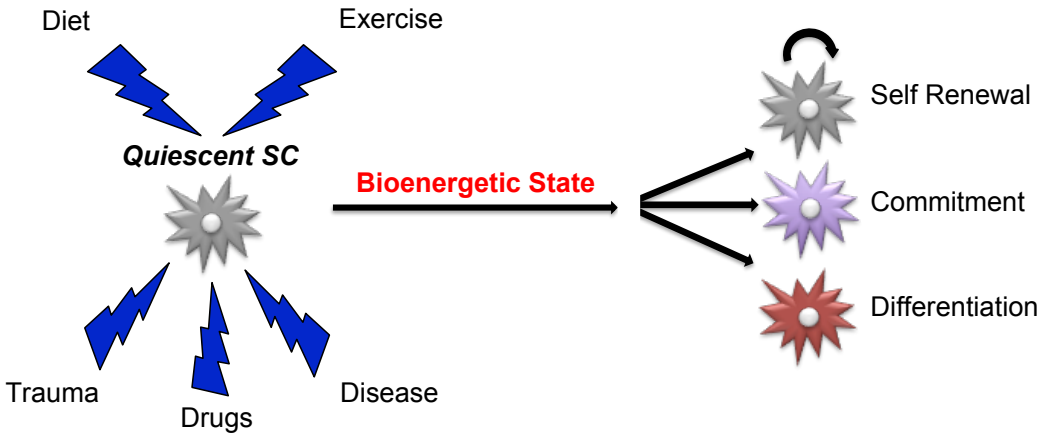

Figure 2. External cues define the metabolic character for how a stem cell will behave when activated. See text for more details.

Figure 3

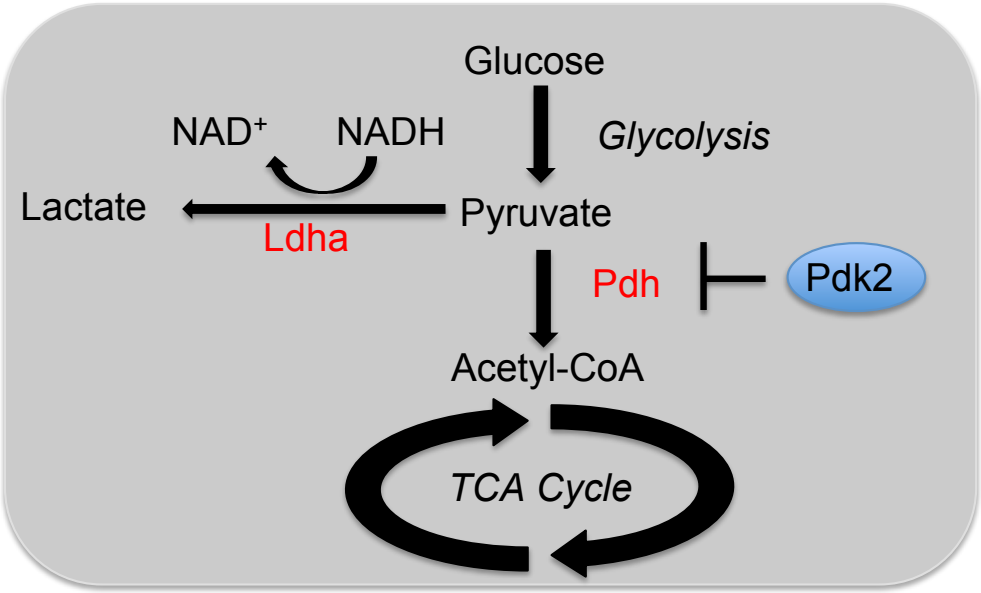

Figure 3. Diagram representing key enzymes in anaerobic glycolysis. See text for more details

Figure 4

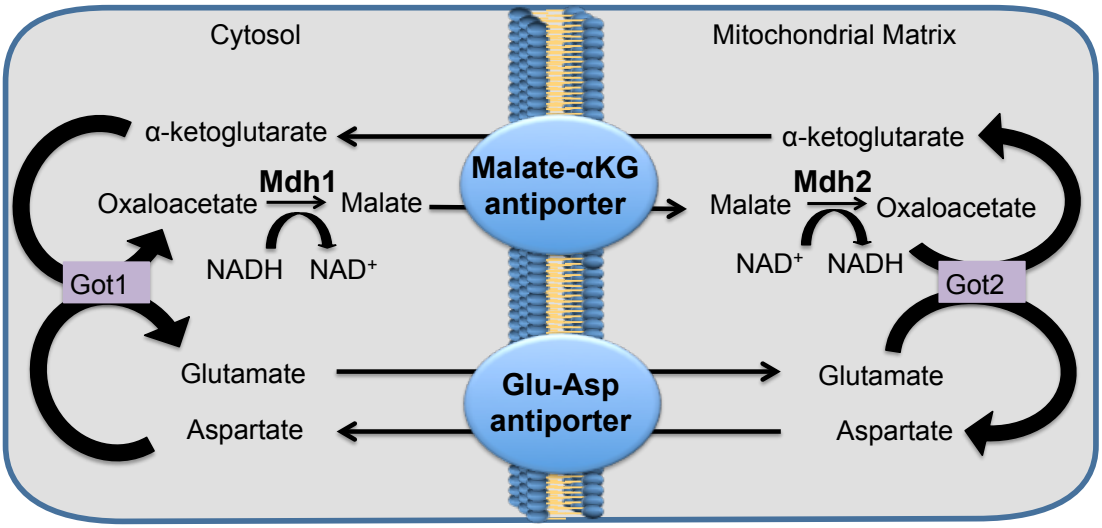

Figure 4. Diagram representing the malate-aspartate shuttle. See text for more detail.

Figure 5

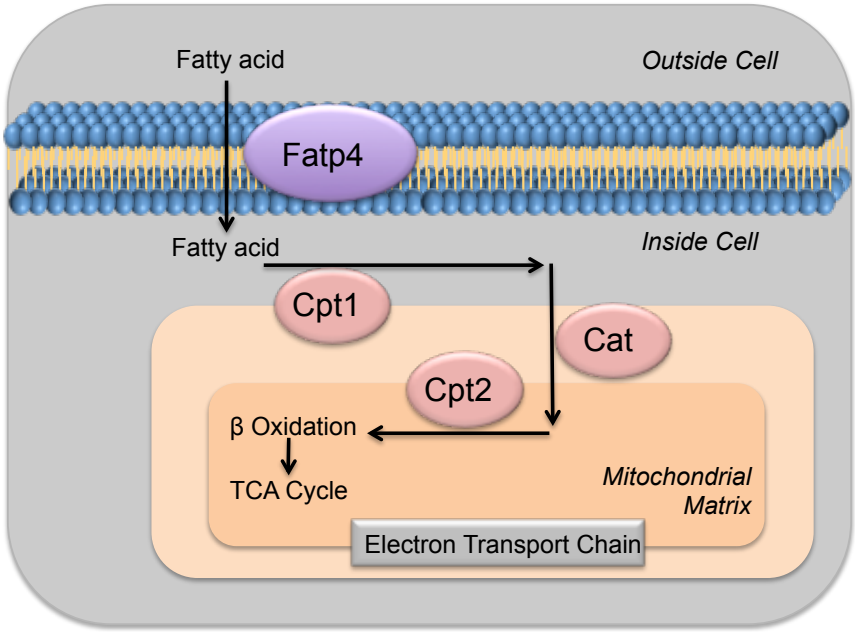

Figure 5. Diagram representing fatty acid transport into the mitochondria. See text for further details.

Figure 6

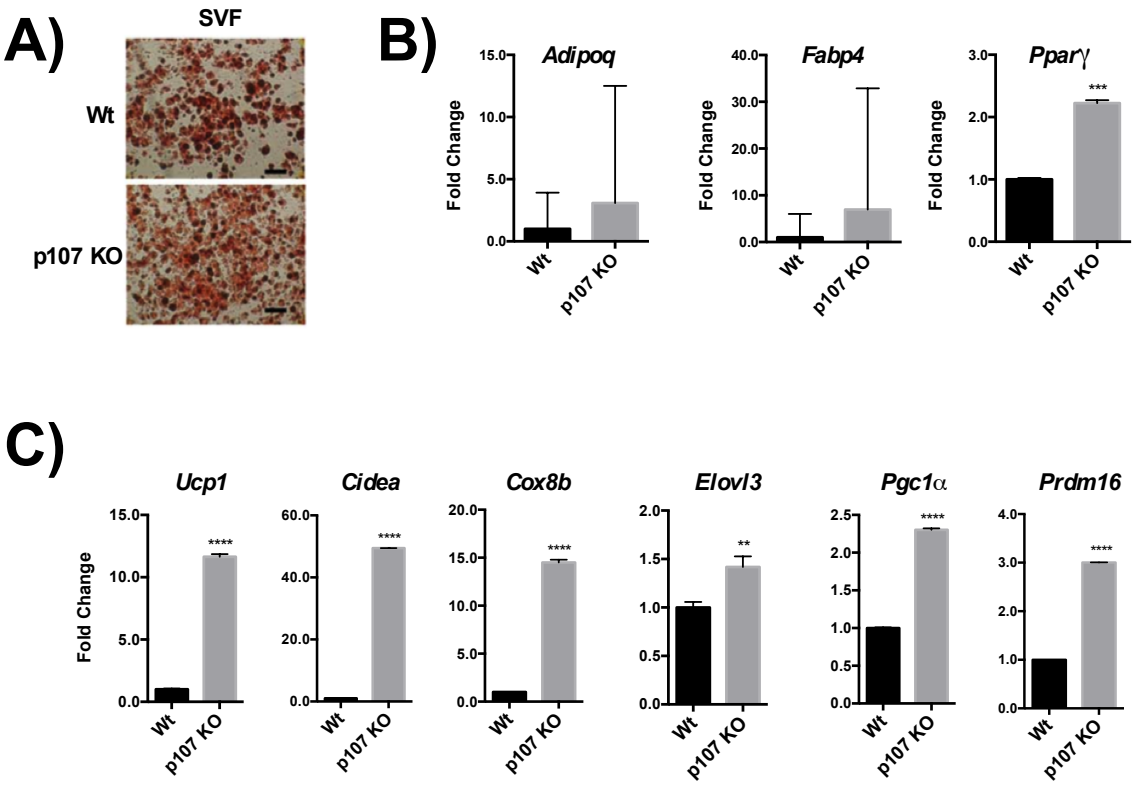

Figure 6. *p107* KO stromal vascular fraction (SVF) cells readily differentiate into brown-type adipocytes. (A) Representative oil Red O staining of Wt and p107 KO SVF cells after 7 days of adipocyte differentiation (scale bar = 250m). **(B)** Gene expression analysis by qPCR for general adipogenic differentiation markers, *Adipoq, Fabp4,* and *Ppar* ($p < .001$), in Wt and p107 KO SVF cells after 7 days of adipocyte differentiation (n=3). **(C)** Gene expression analysis by qPCR for general brown-type adipocyte differentiation markers, *Ucp1*, *Cidea*, *Cox8b*, *Elovl3*, *Pgc-1*, and *Prdm16* after 7 days of adipocyte differentiation of Wt and p107 KO SVF cells (n=3, asterisks denote significance, $**p<0.01$, $****p<0.0001$). All data are mean +/- SD.

Figure 7

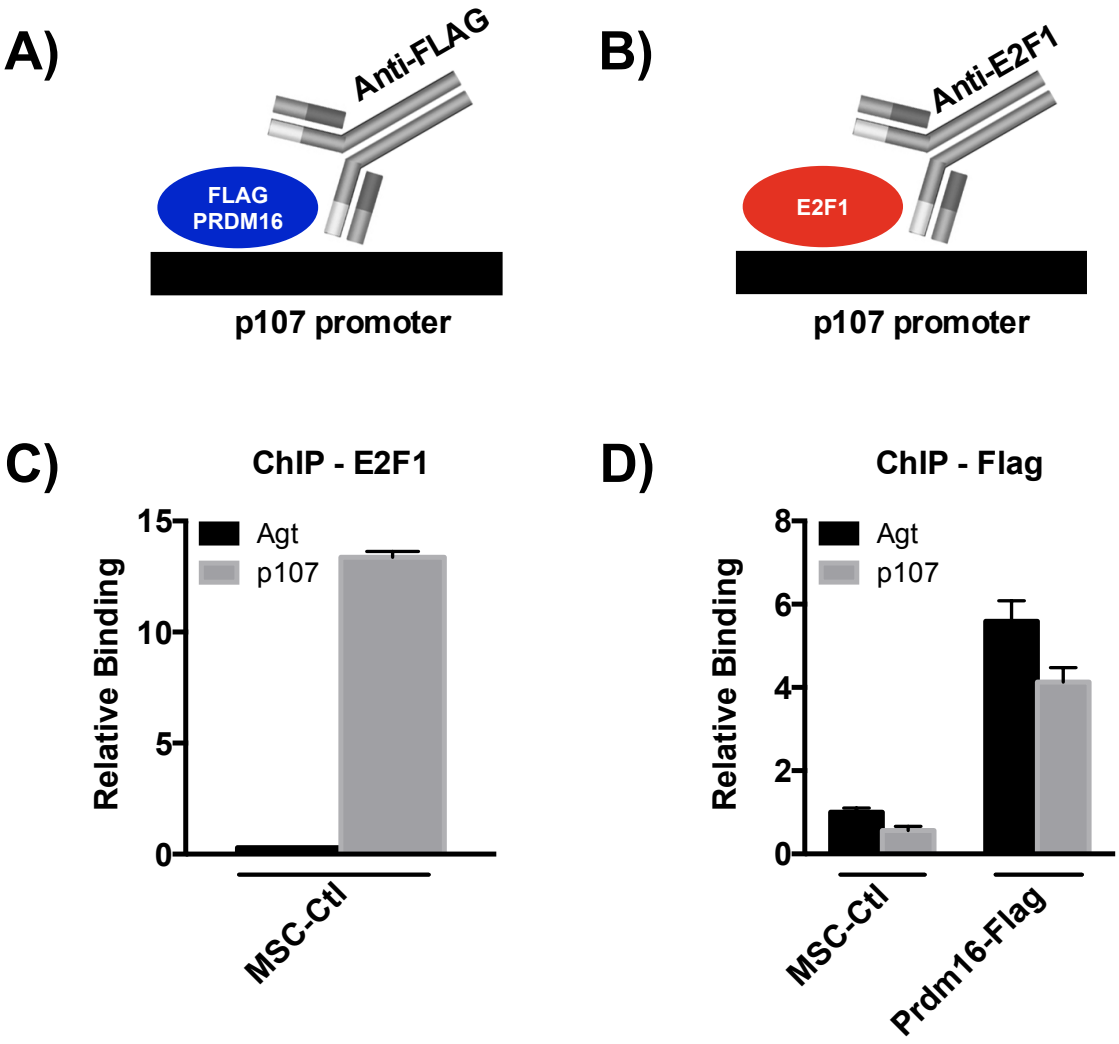

Figure 7. Prdm16 regulates p107 gene expression. (**A**) and **(B)** Diagram showing anti-Flag and E2F1 antibodies interacting with Prdm16 and E2F1, respectively at the p107 promoter. (**C**) Quantitative chromatin immunoprecipitation (qChIP) analysis for E2F1 in MSC-Ctl cells amplified with primers for the gene promoters of p107 or negative control angiotensinogen (Agt). (**D**) qChIP analysis of Flag-tagged Prdm16 in MSC-Ctl and Prdm16-Flag cell lines amplified with primers for the gene promoters of p107 (-214 to -32) or positive control angiotensinogen (Agt) (-127 to +23) (n=3) All data are mean +/- SD. Note that Prdm16 interacts at the p107 promoter.

Figure 8

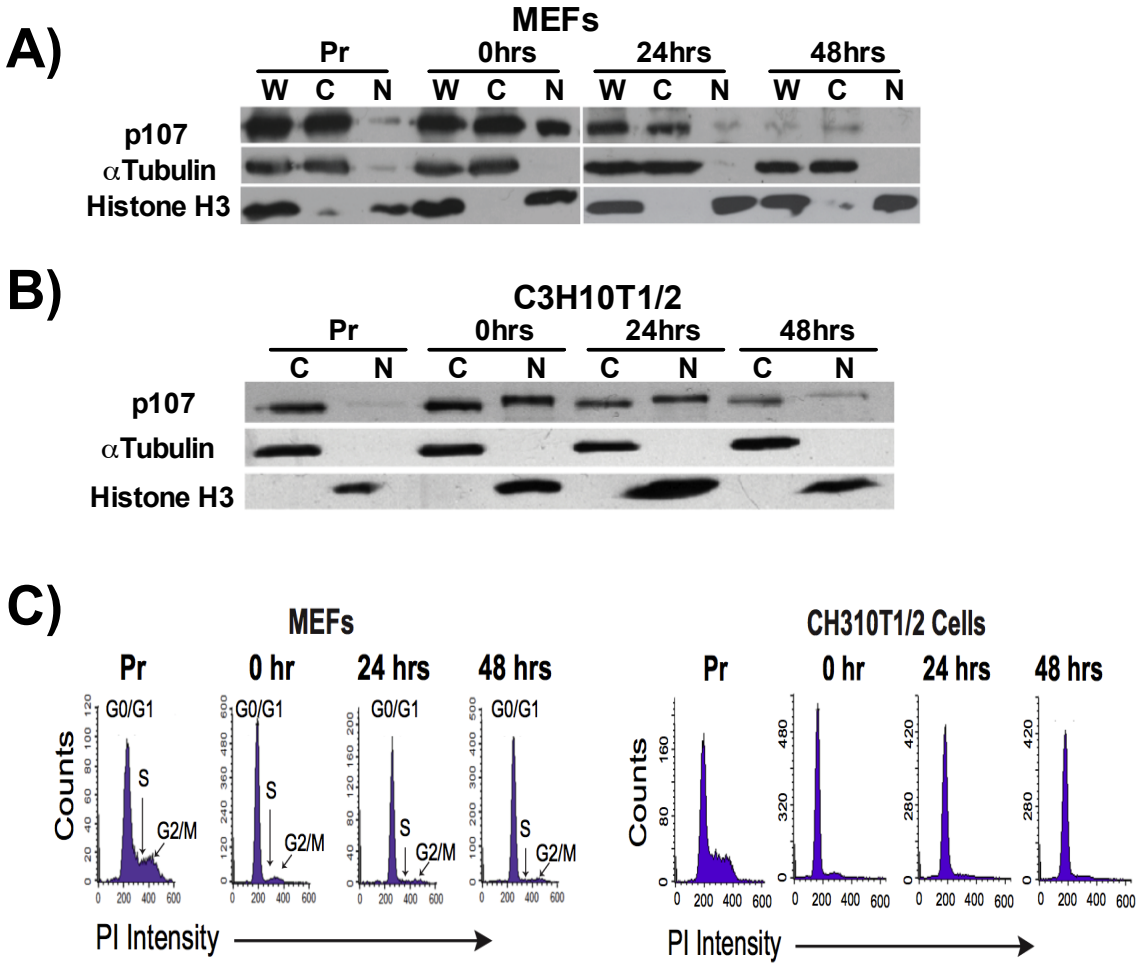

Figure 8. p107 is activated by nuclear translocation in G_0/G_1 (A) Representative Western blot of whole cell (W), cytoplasmic (C), and nuclear (N) fractions for p107, α-Tubulin (cytoplasmic control) and Histone H3 (nuclear control**)** during proliferation (Pr), 0hrs, 24 hours and 48 hours at confluency in Wt MEFs. **(B)** Representative Western blot of C and N fractions for p107, α-Tubulin and Histone H3 during Pr, 0hrs, 24 hours and 48 hours in C3H10T1/2 **(C)** Histograms of MEFs and C3H10T1/2 cells stained with PI and analyzed by flow cytometry during Pr, 0hrs, 24 hours and 48 hours at confluency. The peak areas represent the cell population in G_0/G_1, S and G2/M. Note that when cells reach confluency they are in a G_0/G_1 state.

Figure 9

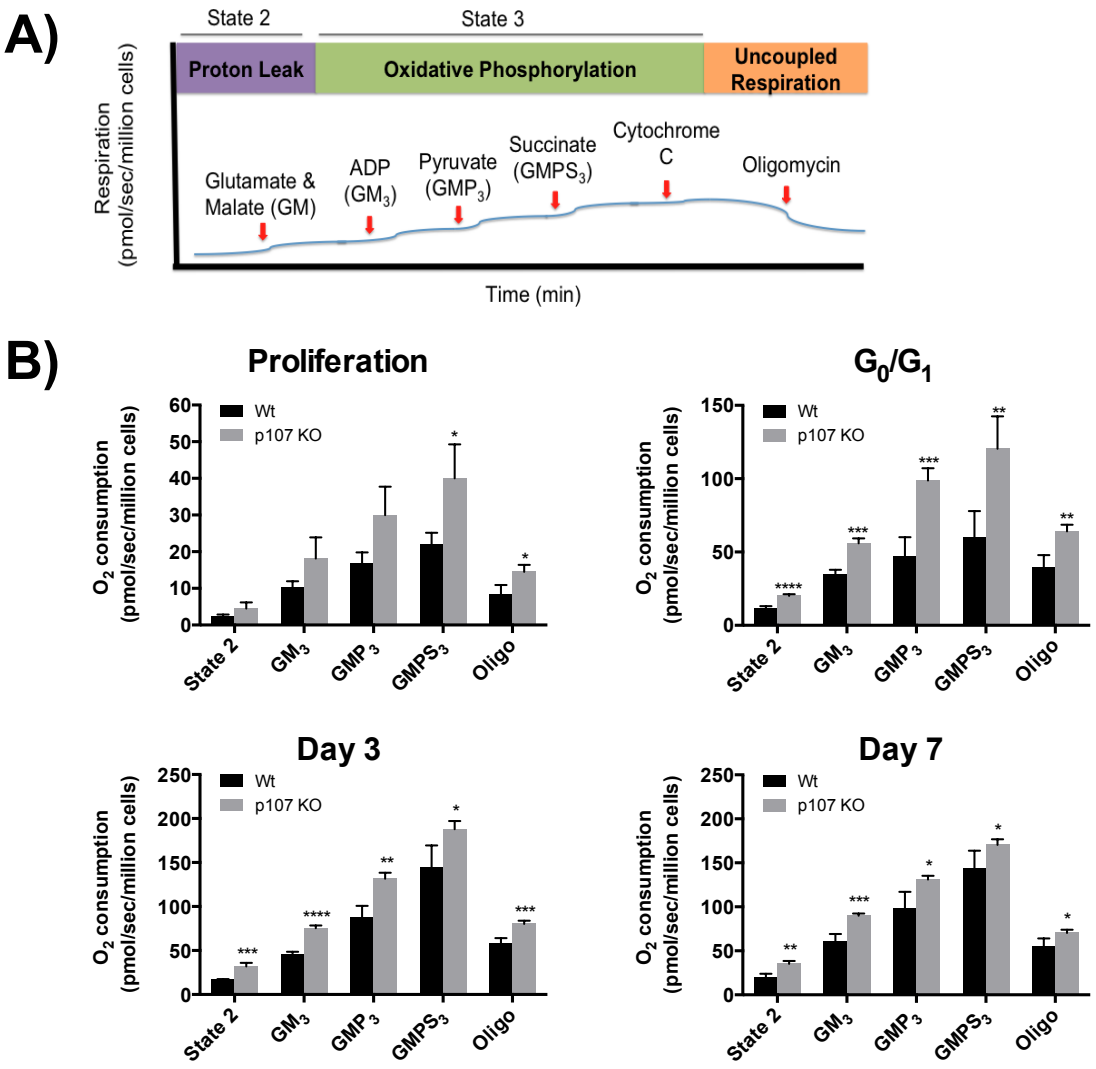

Figure 9. p107 KO MEFs have increased O_2 consumption in G_0/G_1 and differentiation. (**A**) Diagram representing the consecutive addition of substrates to Oroboros Oxygraph-2K (**B**) State 3 respiration reflecting the capacities for oxidative phosphorylation supported by both NADH-generating complex I substrates glutamate and malate **(GM_3)** and together with pyruvate **(GMP_3)** and by $FADH_2$-generating complex II substrates GMP with succinate **($GMPS_3$)**; as well as proton leak assessed during non-ADP dependent respiration (**State 2 respiration**; complex 1 supported by GM before the addition of ADP) and in the presence of oligomycin (**Oligo**) after the

addition of ADP (both complex I and II supported by GMPS) of p107 KO and Wt MEFs during proliferation, G_0/G_1, and Day 3 and Day 7 of adipocyte differentiation. Note genetic deletion of p107 has no effect on mitochondrial oxygen consumption during proliferation (n=3-5, asterisks denote significance, *p<0.05, **p<0.01, ***p<0.001, ****p<0.0001). All data are mean +/- SD.

Figure 10

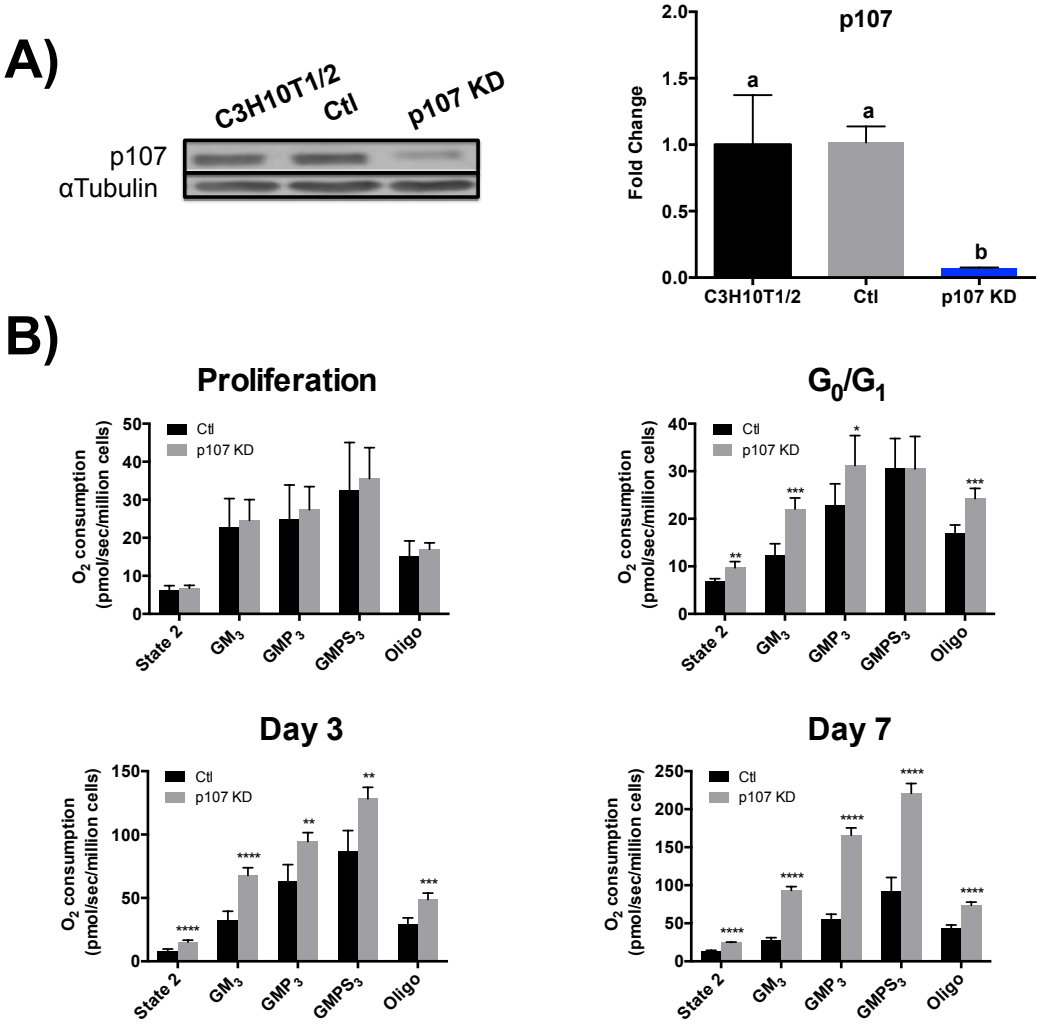

Figure 10. p107 depletion increases O_2 consumption in G_0/G_1 and differentiation (**A**) Representative Western blot and graphical representation of p107 protein levels in C3H10T1/2, Ctl and p107 KD cell lines. (n=4, One-way ANOVA and Tukey Post-hoc test were used, different letters indicate significant difference $p<0.0001$). **(B)** State 3 respiration reflecting the capacities for oxidative phosphorylation supported by both NADH-generating complex I substrates glutamate and malate (GM_3) and together with pyruvate (GMP_3) and by $FADH_2$-generating complex II substrates GMP with succinate ($GMPS_3$); as well as proton leak assessed during non-ADP dependent respiration (**State 2 respiration**; complex 1 suppored by GM before the addition of ADP) and in the presence of oligomycin after the addition of ADP (both complex I and II supported by GMPS) of

Ctl and p107 KD cell lines during proliferation, G_0/G_1, and Day 3 and Day 7 of adipocyte differentiation. Note p107 depletion has no effect on mitochondrial oxygen consumption during growth. (n= 4-5, asterisks denote significance, *p<0.05, **p<0.01, ***p<0.001, ****p<0.0001). All data are mean +/- SD.

Figure 11

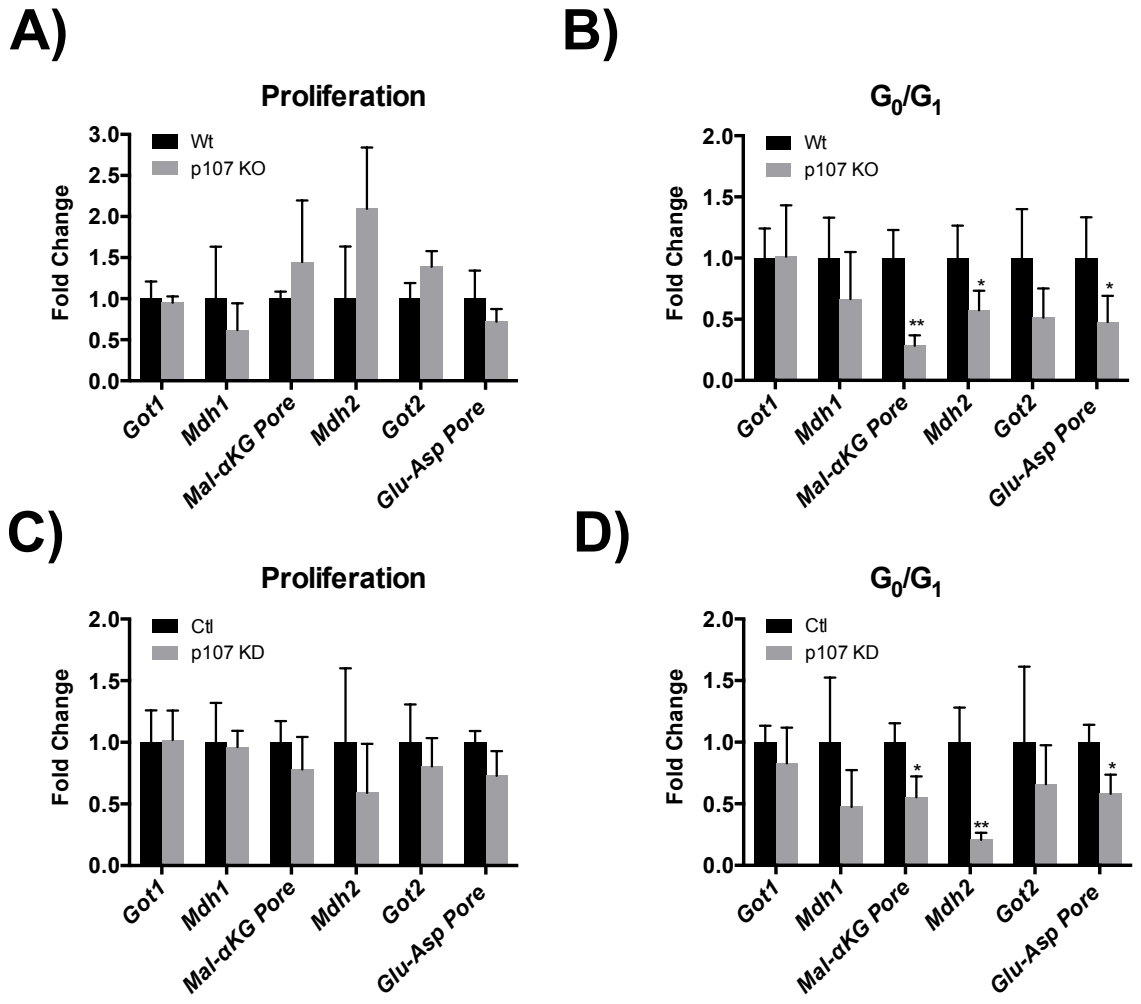

Figure 11. p107-depleted stem cells have altered NADH partitioning in G_0/G_1 (A) Gene expression analysis by qPCR for markers of the Malate-Aspartate shuttle: cytosolic aspartate transaminase (*Got1*), Malate Dehydrogenase 1 *(Mdh1*), Malate-αKetoglutarate Antiporter (*Mal-αKG Pore*), Malate Dehydrogenase 2 *(Mdh2*), mitochondrial aspartate transaminase (*Got2*), and Glutamate-Aspartate Antiporter (*Glu-Asp Pore*), and in Wt and p107 KO MEFs during proliferation and G_0/G_1 (n=3-5, *p<0.05, **p<0.01). **(B)** Gene expression analysis by qPCR for markers of the Malate-Aspartate shuttle as in **(A)** in Ctl and p107 KD cell lines during proliferation and G_0/G_1 (n=3-4, *p<0.05, **p<0.01). All data are mean +/- SD.

Figure 12

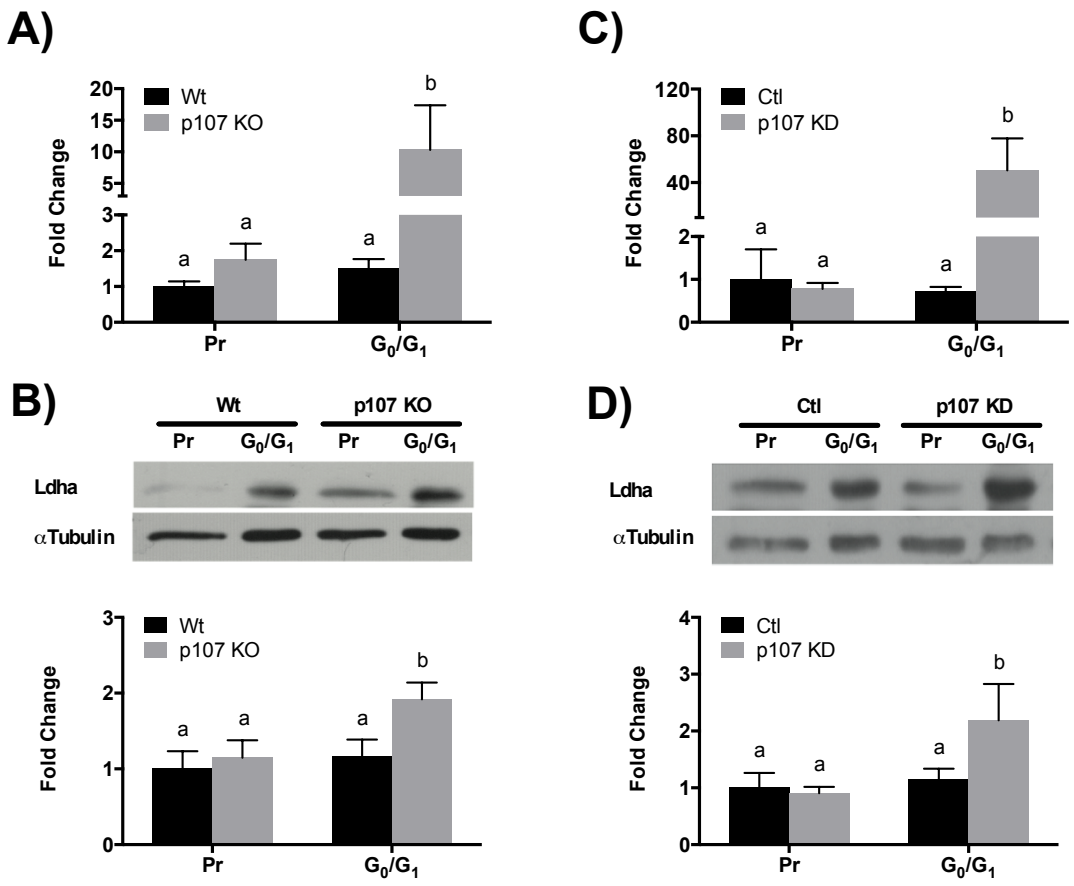

Figure 12. p107-KO and KD stem cells participate in anaerobic glycolysis at G_0/G_1 **(A)** Gene expression analysis by qPCR of lactate dehydrogenase (*Ldha*) in p107 KO and Wt MEFs during proliferation and G_0/G_1 ($p<0.05$). **(B)** Representative western blot and graphical representation of Ldha protein levels in p107 KO and Wt MEFs during proliferation and G_0/G_1 ($p<0.001$). **(C)** Gene expression analysis by qPCR of lactate dehydrogenase (*Ldha*) in Ctl and p107 KD cell lines during Pr and G_0/G_1 ($p<0.01$). **(D)** Representative western blot and graphical representation of Ldha protein levels in Ctl and p107 KD cell lines during proliferation and G_0/G_1 ($p<0.01$). (n=3-4, Two-way ANOVA and Tukey Post-hoc test were used, different letter indicates significant difference).
All data are mean +/- SD.

Figure 13

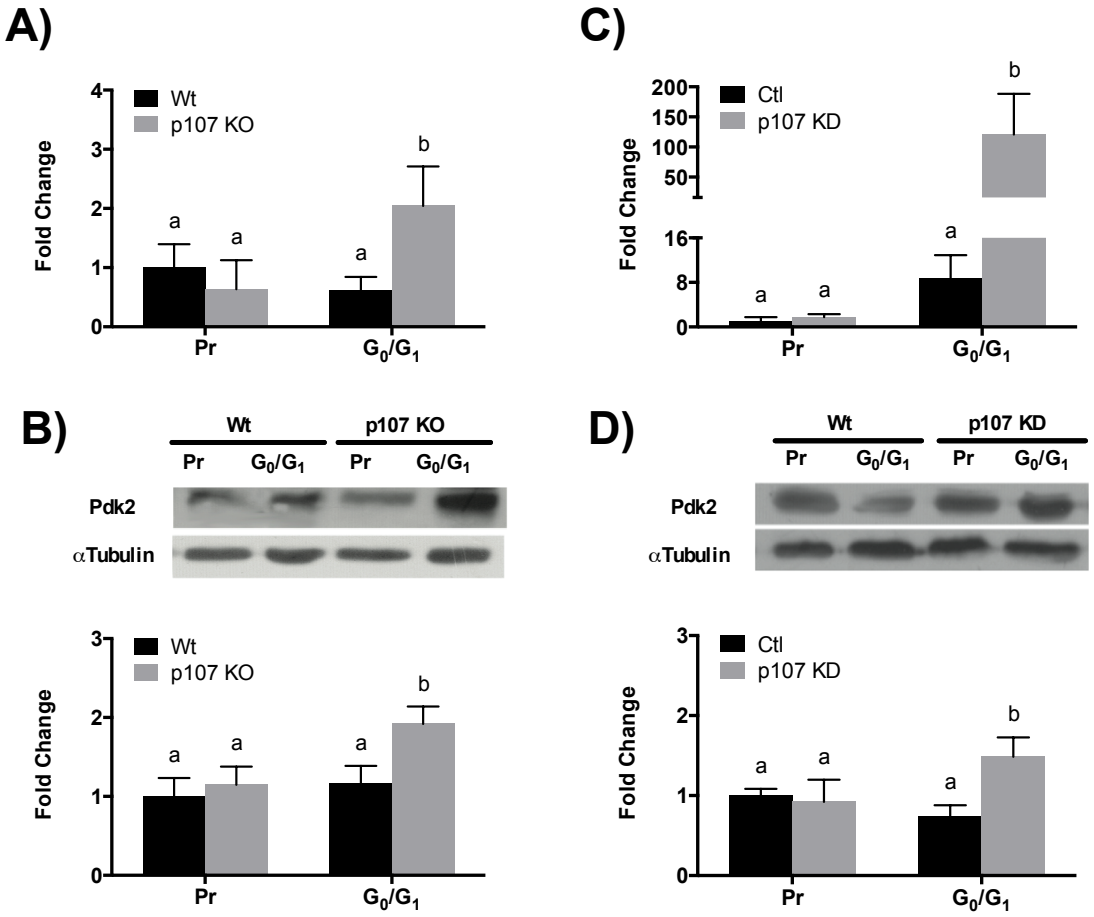

Figure 13. p107-KO and KD stem cells participate in anaerobic glycolysis at G_0/G_1 **(A)** Gene expression analysis by qPCR of pyruvate dehydrogenase (*Pdk2*) in p107 KO and Wt MEFs during proliferation and G_0/G_1 ($p<0.05$). **(B)** Representative western blot and graphical representation of Pdk2 protein levels in p107 KO and Wt MEFs during proliferation and G_0/G_1 ($p<0.001$). **(C)** Gene expression analysis by qPCR of pyruvate dehydrogenase (*Pdk2*) in Ctl and p107 KD cell lines during Pr and G_0/G_1 ($p<0.05$). **(D)** Representative western blot and graphical representation of Pdk2 protein levels in Ctl and p107 KD cell lines during proliferation and G_0/G_1 ($p<0.01$). (n=3-4, Two-way ANOVA and Tukey Post-hoc test were used, different letter indicates significant difference. All data are mean +/- SD.

Figure 14

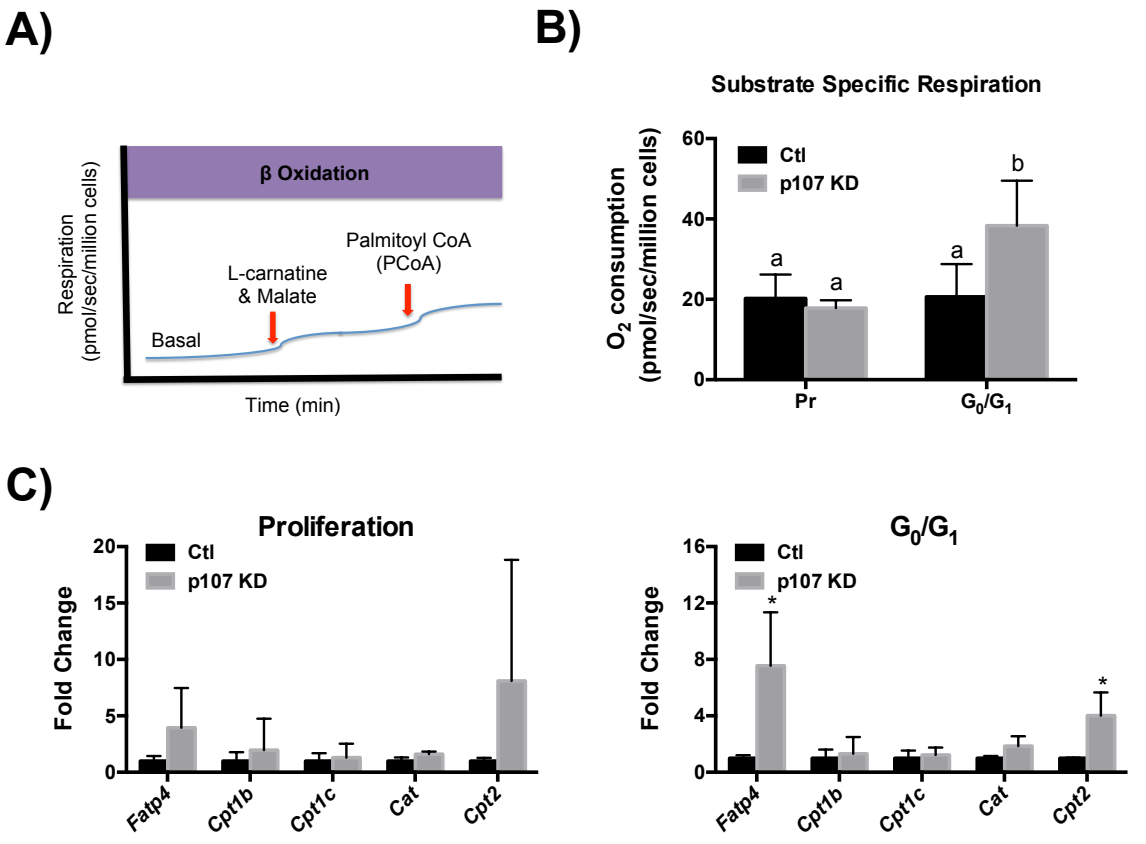

Figure 14. p107 KD cells have enhanced β-oxidation in G_0/G_1 (**A**) Diagram representing the protocol of consecutive addition of substrates to measure fatty acid β-oxidation potential. (**B**) Substrates were added consecutively according to (**A**) and total O_2 consumption was measured in Ctl and p107 KD cell lines during proliferation and G_0/G_1 states (n=4, Two-way ANOVA and Tukey Post-hoc test were used, different letter indicates significant difference, $p<0.05$). (**C**) Gene expression analysis by qPCR for markers of fatty acid transport: Fatty acid transport protein 4 (*Fatp4*), Carnitine palmitoyltransferase 1b (*Cpt1b*), Carnitine palmitoyltransferase 1c (*Cpt1c*), Carnitine-acylcarnitine translocase (*Cat*) and Carnitine palmitoyltransferase 2 (*Cpt2*), in Ctl and p107 KD cell lines during proliferation and G_0/G_1 (n=3, *$p<0.05$).

All data are mean +/- SD.

Figure 15

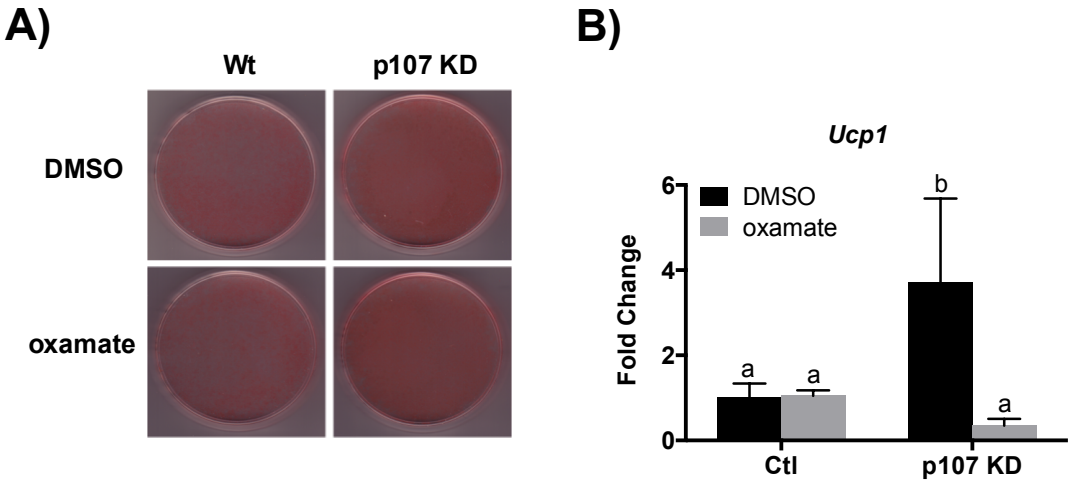

Figure 15. Anaerobic glycolysis in G_0/G_1 is necessary for brown-type differentiation **(A)** Oil Red O staining after 7 days of adipocyte differentiation of Ctl and p107 KD cells treated with DMSO or oxamate. **(B)** Gene expression analysis by qPCR of *Ucp1* after 7 days post differentiation in Ctl and p107 KD cells treated with DMSO or oxamate (n=4-5, Two-way ANOVA and Tukey Post-hoc test were used, different letter indicates significant difference, $p<0.05$. All data are mean +/- SD. Note that inhibition of anaerobic glycolysis via oxamate administration prevented the brown-type differentiation potential of p107 KD stem cells.

Figure 16

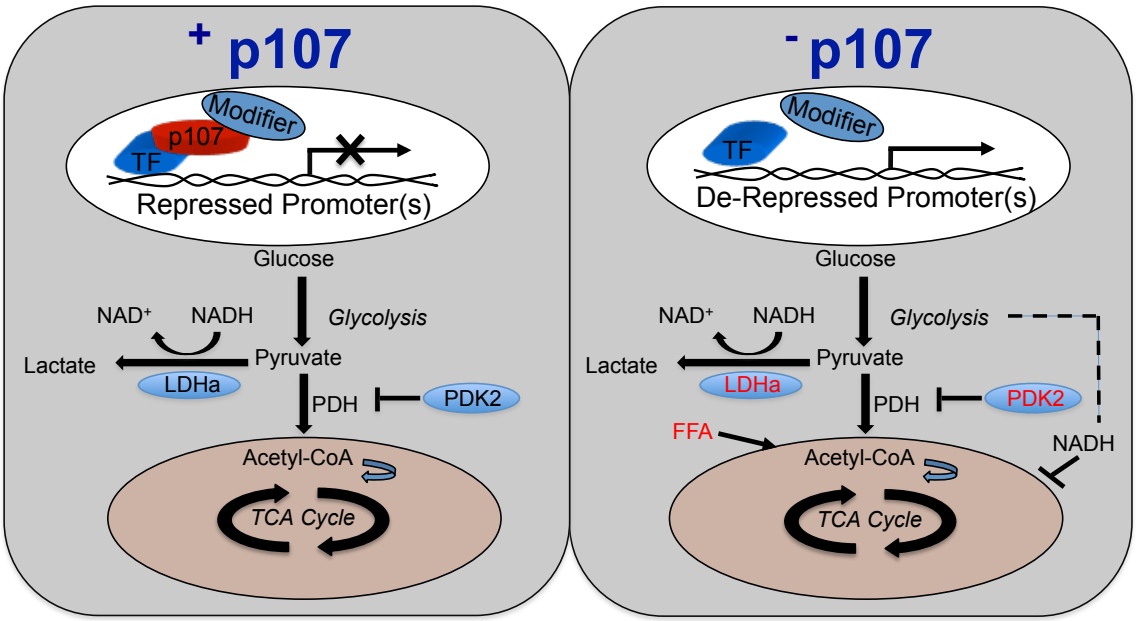

Figure 16. Metabolic reprogramming in the presence or absence of p107. See text for further details.

14. REFERENCES

1. Abumaree, M.H., Al Jumah, M.A., Kalionis, B., Jawdat, D., Al Khaldi, A., Altalabani, A.A., and Knawy, B.A. (2012). Phenotypic and functional characterization of mesenchymal stem cells from chorionic villi of human term placenta. Stem Cell Rev *9*, 16-31.
2. Agathocleous, M. and Harris, W.A. (2013). Metabolism in physiological cell proliferation and differentiation. Trends Cell Biol *23*, 484-92.
3. Ahfeldt, T., Schinzel, R.T., Lee, Y.K., Hendrickson, D., Kaplan, A., Lum, D.H., Camahort, R., Xia, F., Shay, J., Rhee, E.P., Clish, C.B., Deo, R.C., Shen, T., et al. (2012). Programming human pluripotent stem cells into white and brown adipocytes. Nat Cell Biol *14*, 209-219.
4. Arden, C., Tudhope, S.J., Petrie, J.L., Al-Oanzi, Z.H., Cullen, K.S., Lange, A.J., Towle, H.C., and Agius, L. (2012). Fructose 2,6-bisphosphate is essential for glucose-regulated gene transcription of glucose-6-phosphatase and other ChREBP target genes in hepatocytes. Biochem. J. *443*, 111-123.
5. Armstrong, L., Tilgner, K., Saretzki, G., Atkinson, S.P., Stojkovic, M., Moreno, R., Przyborski, S., and Lako, M. (2010). Human induced pluripotent stem cell lines show stress defense mechanisms and mitochondrial regulation similar to those of human embryonic stem cells. Stem Cells *28*,661–673.
6. Bachman, E.S., Dhillon, H., Zhang, C.Y., Cinti, S., Bianco, A.C., Kobilka, B.K., and Lowell, B.B. (2002). BetaAR signaling required for diet-induced thermogenesis and obesity resistance. Science *297*, 843–845.

7. Barbatelli, G., Murano, I., Madsen, L., Hao, Q., Jimenez, M., Kristiansen, K., Giacobino, J.P., De Matteis, R., and Cinti, S. (2010). The emergence of cold-induced brown adipocytes in mouse white fat depots is determined predominantly by white to brown adipocyte transdifferentiation. Am J Physiol Endocrinol Metab *298*, E1244–1253.

8. Bartelt, A., Bruns, O.T., Reimer, R., Hohenberg, H., Ittrich, H., Peldschus, K., Kaul, M.G., Tromsdorf, U.I., Weller, H., Waurisch, C., Eychmüller, A., Gordts, P. L.S.M., Rinninger, F., Bruegelmann, K., Freund, B., Nielsen, P., Merkel, M., Heeren, J. (2011). Brown adipose tissue activity controls triglyceride clearance. Nat Med *17*, 200–205.

9. Brooks, G.A. (2009). Cell-cell and intracellular lactate shuttles. J Physiol *587*, 5591-600.

10. Bernstein, B.E., Mikkelsen, T.S., Xie, X., Kamal, M., Huebert, D.J., Cuff, J., Fry, B., Meissner, A., Wernig, M., Plath, K., et al. (2006). A bivalent chromatin structure marks key developmental genes in embryonic stem cells. Cell *125*,315–326.

11. Boström, P., Wu, J., Jedrychowski, M.P., Korde, A., Ye, L., Lo, J.C., Rasbach, K.A., Boström, E.A., Choi, J.H., Long, J.Z., Kajimura, S., Zingaretti, M.C., Vind, B.F., Tu, H., Cinti, S., Højlund, K., Gygi, S.P., and Spiegelman, B.M. (2012). A PGC1-α-dependent myokine that drives brown-fat-like development of white fat and thermogenesis. Nature *11*, 463-468.

12. Bowers, R.R., Kim, J.W., Otto, T.C., and Lane, M.D. (2006). Stable stem cell commitment to the adipocyte lineage by inhibition of DNA methylation: role of the BMP-4 gene. Proc Natl Acad Sci U S A *103*, 13022–13027.

13. Burkhart, D., and Sage, J. (2008). Cellular mechanisms of tumour suppression by the retinoblastoma gene. Nat Rev Cancer *8*, 671–682.

14. Cai, L., Sutter, B.M., Li, B., and Tu, B.P. (2011). Acetyl-CoA induces cell growth and proliferation by promoting the acetylation of histones at growth genes. Mol Cell *42*, 426–437.

15. Cannon, B., and Nedergaard, J. (2004). Brown adipose tissue: function and physiological significance. Physiol Rev *84*, 277–359.

16. Carrière, A., Jeanson, Y., Berger-Müller, S., André, M., Chenouard, V., Arnaud, E., Barreau, C., Walther, R., Galinier, A., Wdziekonski, B., Villageois, P., Louche, K., Collas, P., Moro, C., Dani, C., Villarroya, F., and Casteilla, L. (2006). Browning of white adipose cells by intermediate metabolites: an adaptive mechanism to alleviate redox pressure. Diabetes. 63, 3253-3265.

17. Cheng, T., Sudderth, J., Yang, C., Mullen, A.R., Jin, E.S., and Matés, J.M. (2011). Pyruvate carboxylase is required for glutamine-independent growth of tumor cells. Proceedings of the National Academy of Sciences *208*, 8674–8679.

18. Chondronikola, M., Volpi, E., Børsheim, E., Porter, C., Annamalai, P., Enerbäck, S., Lidell, M.E., Saraf, M.K., Labbe, S.M., Hurren, N.M., et al. (2014). Brown adipose tissue improves whole body glucose homeostasis and insulin sensitivity in humans. Diabetes *63*, 4089–4099.

19. Choudhary, C., Kumar, C., Gnad, F., Nielsen, M.L., Rehman, M., Walther, T.C., Olsen, J.V., and Mann, M. (2009). Lysine acetylation targets proteins complexes and co-regulates major cell functions. Science 325, 834-840.

20. Cimmino, L., Abdel-Wahab, O., Levine, R.L., and Aifantis, I. (2011). TET family proteins and their role in stem cell differentiation and transformation. Cell Stem Cell *9*, 193–204.

21. Cinti, S. (2002) Adipocyte differentiation and transdifferentation: plasticity of the adipose organ. J Endocrinol Invest *25*, 823-835.

22. Cinti, S. (2005). The adipose organ. Prostaglandins Leukot Essent Fatty Acids *73*, 9–15.

23. Cinti, S. (2006). The role of brown adipose tissue in human obesity. Nutr Metab Cardiovasc Dis *16*, 569–574.

24. Classon, M., Kennedy, B.K., Mulloy, R., and Harlow, E. (2000). Opposing roles of pRB and p107 in adipocyte differentiation. Proc Natl Acad Sci U S A *97*, 10826–10831.

25. Cohen, P., Levy, J.D., Zhang, Y., Frontini, A., Kolodin, D.P., Svensson, K.J., Lo, J.C., Zeng, X., Ye, L., Khandekar, M.J., Wu, J., Gunawardana, S.C., et al. (2014). Ablation of PRDM16 and beige adipose causes metabolic dysfunction and a subcutaneous to visceral fat switch. Cell *16*, 304-316.

26. Cousin, B., Cinti, S., Morroni, M., Raimbault, S., Ricquier, D., Pénicaud, L., and Casteilla, L. (1992). Occurrence of brown adipocytes in rat white adipose tissue: molecular and morphological characterization. J Cell Sci *103*, 931–942.

27. Covas, D.T., Panepucci, R.A., Fontes, A.M., Silva, W.A., Orellana, M.D., et al. (2008). Multipotent mesenchymal stromal cells obtained from diverse human tissues share functional properties and gene-expression profile with CD146+ perivascular cells and fibroblasts. Exp Hematol. *36*, 642-654.

28. Cypess, A.M., Lehman, S., Williams, G., Tal, I., Rodman, D., Goldfine, A.B., Kuo, F.C., Palmer, E.L., Tseng, Y.H., Doria, A., Kolodny, G.M., Kahn, C.R. (2009). Identification and importance of brown adipose tissue in adult humans. N Engl J Med *360*, 1509–1517.

29. Cypess, A.M., White, A.P., Vernochet, C., Schulz, T.J., Xue, R., Sass, C.A., Huang, T.L., Roberts-Toler, C., Weiner, L.S., Sze, C., Chacko, et al. (2013). Anatomical localization, gene expression profiling and functional characterization of adult human neck brown fat. Nat Med *19*, 635-9.

30. Dali-Youcef, N., Mataki, C., Coste, A., Messaddeq, N., Giroud, S., Blanc, S., Koehl, C., Champy, M.F., Chambon, P., Fajas, L., Metzger, D., Schoonjans, K., and Auwerx, J. (2007). Adipose tissue-specific inactivation of the retinoblastoma protein protects against diabesity because of increased energy expenditure. Proc Natl Acad Sci U S A *104*, 10703-10708.

31. De Sousa, M., Porras, D.P., Perry, C.G., Seale, P., and Scimè, A. (2014) p107 is a crucial regulator for determining the adipocyte lineage fate choices of stem cells. Stem Cells *32*, 1323-1336.

32. Diaz-Moralli, S., Ramos-Montoya, A., Marin, S., Fernandez-Alvarez, A., Casado, M. and Cascante, M. (2012). Target metabolomics revealed complementary roles

of hexose- and pentose-phosphates in the regulation of carbohydrate-dependent gene expression. Am J Physiol Endocrinol Metab. *303*, E234–242.

33. Eckfeldt, C.E., Mendenhall, E.M., and Verfaillie, C.M. (2005). The molecular repertoire of the 'almighty' stem cell. Nat Rev Mol Cell Biol *6*, 726-737.

34. Elabd, C., Chiellini, C., Carmona, M., Galitzky, J., Cochet, O., Petersen, R., Pénicaud, L., Kristiansen, K., Bouloumié, A., Casteilla, L., Dani, C., Ailhaud, G., Amri, E.Z. (2009). Human multipotent adipose-derived stem cells differentiate into functional brown adipocytes. Stem Cells *27*, 2753–2760.

35. Elabd, C., Chiellini, C., Massoudi, A., Cochet, O., Zaragosi, L.E., Trojani, C., Michiels, J.F., Weiss, P., Carle, G., Rochet, N., Dechesne, C.A., Ailhaud, G., Dani, C., Amri, E.Z. (2007). Human adipose tissue-derived multipotent stem cells differentiate in vitro and in vivo into osteocyte-like cells. Biochem Biophys Res Commun *361*, 342–348.

36. Enerbäck, S. (2009). The origins of brown adipose tissue. New Engl J Med *360*, 2021–2023.

37. Ewen, M.E., Xing, Y.G., Lawrence, J.B., and Livingston, D.M. (1991). Molecular cloning, chromosomal mapping, and expression of the cDNA for p107, a retinoblastoma gene product-related protein. Cell *66*, 1155–1164.

38. Feldmann, H.M., Golozoubova, V., Cannon, B., and Nedergaard, J. (2009). UCP1 ablation induces obesity and abolishes diet-induced thermogenesis in mice exempt from thermal stress by living at thermoneutrality. Cell Metab *9*, 203–209.

39. Fernie, A.R., Carrari, F., and Sweetlove, L.J. (2004). Respiratory metabolism: glycolysis, the TCA cycle and mitochondrial electron transport. Curr Opin Plant Biol *7*, 254–261.

40. Ferreira, R., Magnaghi-Jaulin, L., Robin, P., Harel-Bellan, A., and Trouche, D. (1998). The three members of the pocket proteins family share the ability to repress E2F activity through recruitment of a histone deacetylase. Proc Natl Acad Sci U S A *95*, 10493-10498.

41. Figueroa, M.E., Abdel-Wahab, O., Lu, C., Ward, P.S., Patel, J., Shih, A., Li, Y., Bhagwat, N., Vasanthakumar, A., Fernandez, H.F., Tallman, M.S., Sun, Z., Wolniak, K., Peeters, J.K., et al. (2010). Leukemic IDH1 and IDH2 mutations result in a hypermethylation phenotype, disrupt TET2 function, and impair hematopoietic differentiation. Cancer Cell *18*, 553-67.

42. Fitzgibbons, T.P., Kogan, S., Aouadi, M., Hendricks, G.M., Straubhaar, J., and Czech, M.P. (2011). Similarity of mouse perivascular and brown adipose tissues and their resistance to diet-induced inflammation. Am J Physiol Heart Circ Physiol *301*, H1425–37.

43. Folmes, C.D., Dzeja, P.P., Nelson, T.J. and Terzic, A. (2012). Metabolic plasticity in stem cell homeostasis and differentiation. Cell Stem Cell. 11, 596-606.

44. Folmes, C.D., Nelson, T.J., Martinez-Fernandez, A., Arrell, D.K., Lindor, J.Z., Dzeja, P.P., Ikeda, Y., Perez-Terzic, C., and Terzic, A. (2011a). Somatic oxidative bioenergetics transitions into pluripotency-dependent glycolysis to facilitate nuclear reprogramming. Cell Metab *14*, 264-271.

45. Folmes, C.D., Nelson, T.J., and Terzic, A. (2011b). Energy metabolism in nuclear reprogramming. Biomark Med *5*, 715-29.

46. Friis, R.M., Wu, B.P., Reinke, S.N., Hockman, D.J., Sykes, B.D., and Schultz, M.C. (2009). A glycolytic burst drives glucose induction of global histone acetylation by picNuA4 and SAGA. Nucleic Acids Res *37*, 3969–3980.

47. Frolov, M.V., Dyson, N.J. (2004). Molecular mechanisms of E2F-dependent activation and pRB-mediated repression. J Cell Sci *117*, 2173-2181.

48. Frontini, A., and Cinti, S. (2010). Distribution and development of brown adipocytes in the murine and human adipose organ. Cell Metab *11*, 253-256.

49. Frühbeck, G., Becerril, S., Sáinz, N., Garrastachu, P., and García-Velloso, M.J. (2009). BAT: a new target for human obesity? Trends in Pharmacological Sciences *30*, 387–396.

50. Gesta, S., Tseng, Y.H., and Kahn, C.R. (2007). Developmental origin of fat: Tracking obesity to its source. Cell *131*:242–256.

51. Guppy, M., Greiner, E., and Brand, K. (1993). The role of the Crabtree effect and an endogenous fuel in the energy metabolism of resting and proliferating thymocytes. Eur J Biochem. *212*, 95-99.

52. Hamann, A., Benecke, H., Le Marchand-Brustel, Y., Susulic, V.S., Lowell, B.B., and Flier, J.S. (1995). Characterization of insulin resistance and NIDDM in transgenic mice with reduced brown fat. Diabetes *44*, 1266–1273.

53. Hamann, A., Flier, J.S., and Lowell, B.B. (1996). Decreased brown fat markedly enhances susceptibility to diet-induced obesity, diabetes, and hyperlipidemia. Endocrinology *137*, 21–29.

54. Hannon, G.J., Demetrick, D., and Beach, D. (1993). Isolation of the Rb-related p130 through its interaction with CDK2 and cyclins. Genes & Development *7*, 2378–2391.

55. Hansen, J.B., and Kristiansen, K. (2006). Regulatory circuits controlling white versus brown adipocyte differentiation. The Biochemical Journal *398*, 153–168.

56. Harms, M., and Seale, P. (2013). Brown and beige fat: development, function and therapeutic potential. Nat Med *10*, 1252-1263.

57. Hashimoto, T., Hussien, R., Cho, H.S., Kaufer, D., and Brooks, G.A. (2008). Evidence for a mitochondrial lactate oxidation complex in rat neurons: a crucial component for a brain lactate shuttle. PloS One 3, e2915.

58. Hashimoto, T., Hussien, R., Oommen, S., Gohil, K., and Brooks, G.A. (2007). Lactate sensitive transcription factor network in L6 myocytes: activation of MCT1 expression and mitochondrial biogenesis. FASEB J 21, 2602–2612.

59. Himms-Hagen, J., Melnyk, A., Zingaretti, M.C., Ceresi, E., Barbatelli, G., and Cinti, S. (2000). Multilocular fat cells in WAT of CL-316243-treated rats derive directly from white adipocytes. Am J Physiol Cell Physiol. *279*, C670-681.

60. Hirsch, J., and Batchelor, B. (1976). Adipose tissue cellularity in human obesity. Clin Endocrinol Metab *5*, 299-311.

61. Hotamisligil, G.S., Murray, D.L., Choy, L.N., and Spiegelman, B.M. (1994). Tumor necrosis factor alpha inhibits signaling from the insulin receptor. Proc Natl Acad Sci U S A *91*, 4854-4858.

62. Hu, H.H., Tovar, J.P., Pavlova, Z., Smith, M.L., and Gilsanz, V. (2012). Unequivocal identification of brown adipose tissue in a human infant. Journal of Magnetic Resonance Imaging *35*, 938–942.

63. Ishibashi, J., and Seale, P. (2010). Beige can be slimming. Science *328*, 1113–1114.

64. Ito, K., Carracedo, A., Weiss, D., Arai, F., Ala, U., Avigan, D.E., Schafer, Z.T., Evans, R.M., Suda, T., Lee, C.H., and Pandolfi, P.P. (2012). PPAR pathway for fatty acid oxidation regulates hematopoietic stem cell maintenance. Nature Med. *18*, 1350-1358.

65. Jakus, P.B., Sandor, A., Janaky, T., and Farkas, V. (2008). Cooperation between BAT and WAT of rats in thermogenesis in response to cold, and the mechanism of glycogen accumulation in BAT during reacclimation. Journal of Lipid Research *49*, 332–339.

66. Kaelin, W.G., Jr and McKnight, S.L. (2013). Influence of metabolism on epigenetics and disease. Cell. *153*, 56-69.

67. Kajimura, S., Seale, P., Kubota, K., Lunsford, E., Frangioni, J.V., Gygi, S.P., and Spiegelman, B.M. (2009). Initiation of myoblast to brown fat switch by a PRDM16-C/EBP-beta transcriptional complex. Nature *460*, 1154–1158.

68. Kajimura, S., Seale, P., and Spiegelman, B.M. (2010). Transcriptional control of brown fat development. Cell Metabolism *11*, 257–262.

69. Kajimura, S., Seale, P., Tomaru, T., Erdjument-Bromage, H., Cooper, M.P., Ruas, J.L., Chin, S., Tempst, P., Lazar, M.A. and Spiegelman, B.M. (2008). Regulation

of the brown and white fat gene programs through a PRDM16/CtBP transcriptional complex. Genes Dev. *22*,1397–1409.

70. Kennedy, B. K., Barbie, D. A., Classon, M., Dyson, N., and Harlow, E. (2000). Nuclear organization of DNA replication in primary mammalian cells. Genes & Development *14*, 2855–2868.

71. Kershaw, E.E., and Flier, J.S. (2004). Adipose tissue as an endocrine organ. J Clin Endocrinol Metab *144*, 3765-3773.

72. Lafontan, M. (2008). Advances in adipose tissue metabolism. International Journal of Obesity *32*, S39–51.

73. Landsberg, R.L., Sero, J.E., Danielian, P.S., Yuan, T.L., Lee, E.Y., Lees, J.A. (2003). The role of E2F4 in adipogenesis is independent of its cell cycle regulatory activity. Proc Natl Acad Sci U S A. *100*, 2456-2461.

74. Lange, C. and Calegari, F. (2010). Cdks and cyclins link G1 length and differentiation of embryonic, neural and hematopoietic stem cells. Cell Cycle *9*, 1893–1900.

75. Lean, M.E., James, W.P., Jennings, G., and Trayhurn, P. (1986). Brown adipose tissue uncoupling protein content in human infants, children and adults. Clinical Science *71*, 291–297.

76. Lee, P., Greenfield, J.R., Ho, K.K., and Fulham, M.J. (2010). A critical appraisal of the prevalence and metabolic significance of brown adipose tissue in adult humans. Am J Physiol Endocrinol Metab *299*, E601-606.

77. Lee, W.H., Bookstein, R., Hong, F., Young, L.J., Shew, J.Y., and Lee, E.Y. (1987). Human retinoblastoma susceptibility gene: cloning, identification, and sequence. Science *235*, 1394–1399.

78. Lee, Y.H., Petkova, A.P., Mottillo, E.P., and Granneman, J.G. (2012). In Vivo Identification of Bipotential Adipocyte Progenitors Recruited by β3-Adrenoceptor Activation and High-Fat Feeding. Cell Metabolism *15*, 480–491.

79. Lefterova, M.I., and Lazar, M.A. (2009). New developments in adipogenesis. Trends Endocrinol Metab *20*, 107-114.

80. Lepper, C., and Fan, C.M. (2010). Inducible lineage tracing of Pax7-descendant cells reveals embryonic origin of adult satellite cells. Genesis *48*, 424-436.

81. Li, Y., Graham, C., Lacy, S., Duncan, A.M., and Whyte, P. (1993). The adenovirus E1A-associated 130-kD protein is encoded by a member of the retinoblastoma gene family and physically interacts with cyclins A and E. Genes & Development *7*, 2366–2377.

82. Lidell, M.E., Betz, M.J., Dahlqvist Leinhard, O., Heglind, M., Elander, L., Slawik, M., Mussack, T., Nilsson, D., Romu, T., Nuutila, P., Virtanen, K.A., Beuschlein, F., Persson, A., Borga, M., and Enerbäck, S. (2013). Evidence for two types of brown adipose tissue in humans. Nat Med *19*, 631-634.

83. Lin, C.S, Xin, Z.C., Deng, C.H., Ning, H., Lin, G, and Lue, T.F. (2010). Defining adipose tissue-derived stem cells in tissue and in culture. Histol Histopathol. 25, 807-815.

84. Liu, Y., and Ma, T. (2014). Metabolic regulation of mesenchymal stem cell in expansion and therapeutic application. Biotechnol Prog. [Epub ahead of print]

85. Liu, Z.J., Zhuge, Y., and Velazquez, O.C. (2009). Trafficking and differentiation of mesenchymal stem cells. Journal of Cellular Biochemistry *106*, 984–991.

86. Lopaschuk, G.D., Ussher, J.R., Folmes, C.D., Jaswal, J.S. and Stanley, W.C. (2010). Myocardial fatty acid metabolism in health and disease. Physiol Rev., *90*, 207-258.

87. Lowell, B.B., S-Susulic, V., Hamann, A., Lawitts, J.A., Himms-Hagen, J., Boyer, B.B., Kozak, L.P., and Flier, J.S. (1993). Development of obesity in transgenic mice after genetic ablation of brown adipose tissue. Nature *366*, 740–742.

88. Loyer, P., Cariou, S., Glaise, D., Bilodeau, M., Baffet, G., and Guguen-guillouzo, C. (1996). Growth factor dependence of progression through G1 and S Phases of adult rat hepatocytes in vitro. The Journal of Biological Chemistry *271*, 11484–11492.

89. Lu, C., Ward, P.S., Kapoor, G.S., Rohle, D., Turcan, S., Abdel-Wahab, O., Edwards, C.R., Khanin, R., Figueroa, M.E., Melnick, A., Wellen, K.E., O'Rourke, D.M. et al. (2012). IDH mutation impairs histone demethylation and results in a block to cell differentiation. Nature. *483*, 474-478.

90. Lunt, S.Y. and Vander Heiden, M.G. (2011). Aerobic glycolysis: meeting the metabolic requirements of cell proliferation. Annu Rev Cell Dev Biol *27*,441-464.

91. Ma, S., Yu, H., Zhao, Z., Luo, Z., Chen, J., Ni, Y., Jin, R., Ma, L., Wang, P., Zhu, Z., et al. (2012). Activation of the cold-sensing TRPM8 channel triggers UCP1-dependent thermogenesis and prevents obesity. Journal of Molecular Cell Biology *4*, 88–96.

92. Macaluso, M., Montanari, M., and Giordano, A. (2006). Rb family proteins as modulators of gene expression and new aspects regarding the interaction with chromatin remodeling enzymes. Oncogene 25, 5263-5267.

93. MacDougald, O.A., Lane, M.D. (1995). Transcriptional regulation of gene expression during adipocyte differentiation. Annu Rev Biochem. 64, 345-373.

94. McGarry, J.D., and Brown, N.F. (1997). The mitochondrial carnitine palmitoyltransferase system. From concept to molecular analysis. Eur J Biochem *244*, 1–14.

95. Manning, A.L., and Dyson, N.J. (2011). pRB, a tumor suppressor with a stabilizing presence. Trends in Cell Biology. *21*, 433–441.

96. Martin, C. and Zhang, Y. (2005). The diverse functions of histone lysine methylation. Nature reviews. Molecular cell biology *6***,** 838-849.

97. Matsushita, M., Yoneshiro, T., Aita, S., Kameya, T., Sugie, H., and Saito, M. (2014). Impact of brown adipose tissue on body fatness and glucose metabolism in healthy humans. Int J Obes *38*, 812-817.

98. May, J.S., Prince, A.M., Lyle, R.E., and McGehee, R.E. Jr. (2001). Antisense suppression of p107 inhibits 3T3-L1 adipocyte differentiation. Biochem Biophys Res Commun. *283*, 837–842.

99. Metukuri, M.R., Zhang, P., Basantani, M.K., Chin, C., Stamateris, R.E., Alonso, L.C., Takane, K.K., Gramignoli, R., Strom, S.C., O'Doherty, R.M. et al. (2012). ChREBP mediates glucose-stimulated pancreatic β-cell proliferation. Diabetes. *61*, 2004-15.

100. Mohamed-Ali, V., Goodrick, S., Rawesh, A., Katz, D.R., Miles, J.M., Yudkin, J.S., Klein, S., and Coppack, S.W. (1997). Subcutaneous adipose tissue releases interleukin-6, but not tumor necrosis factor-alpha, in vivo. J Clin Endocrinol Metab *82*, 4196-4200.

101. Muller, H., Bracken, A.P., Vernell, R., Moroni, M.C., Christians, F., Grassilli, E., Prosperini, E., Vigo, E., Oliner, J.D., and Helin, K. (2001). E2Fs regulate the expression of genes involved in differentiation, development, proliferation, and apoptosis. Genes Dev *15*, 267-285.

102. Muoio, D.M., and Newgard, C.B. (2006). Obesity-related derangements in metabolic regulation. Annu Rev Biochem *75*, 367-401.

103. Nicolas, E., Roumillac, C., and Trouche, D. (2003). Balance between acetylation and methylation of histone H3 lysine 9 on the E2F-responsive dihydrofolate reductase promoter. Mol Cell Biol. 23, 1614-1622.

104. Nishio, M., Yoneshiro, T., Nakahara, M., Suzuki, S., Saeki, K., Hasegawa, M., Kawai, Y., Akutsu, H., Umezawa, A., Yasuda, K., Tobe, K., You, A., Kubota, K., Saito, M., and Saeki, K. (2012). Production of functional classical brown adipocytes from human pluripotent stem cells using specific hemopoietin cocktail without gene transfer. Cell Metab *16*, 394-406.

105. Ochocki, J.D., and Simon, M.C. (2013). Nutrient-sensing pathways and metabolic regulation in stem cells. J Cell Biol. *203*, 23–33.

106. Orava, J., Nuutila, P., Lidell, M.E., Oikonen, V., Noponen, T., Viljanen, T., Scheinin, M., Taittonen, M., Niemi, T., Enerbäck, S., and Virtanen, K.A. (2011).

Different metabolic responses of human brown adipose tissue to activation by cold and insulin. Cell Metab *14*, 272-279.

107. Orford, K.W. and Scadden, D.T. (2008). Deconstructing stem cell self-renewal: Genetic insights into cell-cycle regulation. Nat Rev Genet *9*, 115–128.

108. Otto, T.C., and Lane, M.D. (2005). Adipose development: from stem cell to adipocyte. Crit Rev Biochem Mol Biol *40*, 229-242.

109. Ouellet, V., Labbé, S.M., Blondin, D.P., Phoenix, S., Guérin, B., Haman, F., Turcotte, E.E., Richard, D., and Carpentier, A. C. (2012). Brown adipose tissue oxidative metabolism contributes to energy expenditure during acute cold exposure in humans. Journal of Clinical Investigation *122*, 545–552.

110. Panopoulos, A.D., Yanes, O., Ruiz, S., Kida, Y.S., Diep, D., Tautenhahn, R., Herrerias, A., Batchelder, E.M., Plongthongkum, N., Lutz, M., Berggren, W.T., Zhang, K., Evans, R.M., Siuzdak, G., and Belmonte, J.C.I. (2012). The metabolome of induced pluripotent stem cells reveals metabolic changes occurring in somatic cell reprogramming. Cell Res. *22*, 168–177.

111. Park, W., Kim, W.K., and Bae, K.H. (2014). Distinction of white, beige and brown adipocytes derived from mesenchymal stem cells. World J Stem Cells *26*, 33-42.

112. Perwitz, N., Wenzel, J., Wagner, I., Büning, J., Drenckhan, M., Zarse, K., Ristow, M., Lilienthal, W., Lehnert, H., and Klein, J. (2010). Cannabinoid type 1 receptor blockade induces transdifferentiation towards a brown fat phenotype in white adipocytes. Diabetes, Obesity & Metabolism *12*, 158–166.

113. Petrovic, N., Walden, T.B., Shabalina, I.G., Timmons, J.A., Cannon, B., and Nedergaard, J. (2010). Chronic peroxisome proliferator-activated receptor gamma (PPARgamma) activation of epididymally derived white adipocyte cultures reveals a population of thermogenically competent, UCP1-containing adipocytes molecularly distinct from classic brown adipocytes. J Biol Chem. *285*, 7153–7164.

114. Pfeiffer, T., Schuster, S., and Bonhoeffer, S. (2001). Cooperation and competition in the evolution of ATP-producing pathways. Science *292*, 504–507.

115. Pinto, L., Mader, M. T., Irmler, M., Gentilini, M., Santoni, F., Drechsel, D., Blum, R., Stahl, R., Bulfone, A., Malatesta, P., Beckers, J. and Götz, M. (2008). Prospective isolation of functionally distinct radial glial subtypes-lineage and transcriptome analysis. Molecular and Cellular Neurosciences *38*, 15–42.

116. Prigione, A., Lichtner, B., Kuhl, H., Struys, E.A., Wamelink, M., Lehrach, H., Ralser, M., Timmermann, B., and Adjaye, J. (2011). Human induced pluripotent stem cells harbor homoplasmic and heteroplasmic mitochondrial DNA mutations while maintaining human embryonic stem cell-like metabolic reprogramming. Stem Cells. *29*, 1338–1348.

117. Rayman, J.B., Takahashi, Y., Indjeian, V.B., Dannenberg, J.H., Catchpole, S., Watson, R.J., te Riele, H., and Dynlacht, B.D. (2002). E2F mediates cell cycle-dependent transcriptional repression in vivo by recruitment of an HDAC1/mSin3B corepressor complex. Genes Dev.*16*, 933-47.

118. Richon, V.M., Lyle, R.E., and McGehee, R.E. Jr. (1997). Regulation and expression of retinoblastoma proteins p107 and p130 during 3T3-L1 adipocyte differentiation. J Biol Chem *272*, 10117–10124.

119. Rodriguez, A.M., Elabd, C., Amri, E.Z., Ailhaud, G., and Dani, C. (2005). The human adipose tissue is a source of multipotent stem cells. Biochimie *87*, 125–128.

120. Roh, T.Y., Cuddapah, S., and Zhao, K. (2005). Active chromatin do- mains are defined by acetylation islands revealed by genome-wide mapping. Genes Dev. *19,* 542–552.

121. Rosen, E.D., and MacDougald, O.A. (2006). Adipocyte differentiation from the inside out. Nat Rev Mol Cell Biol. *7*, 885-896.

122. Rosen, E.D., and Spiegelman, B.M. (2006). Adipocyte as regulators of energy balance and glucose homeostasis. Nature *444*, 847-853.

123. Rosen, E.D., Walkey, C.J., Puigserver, P., and Spiegelman, B.M. (2000). Transcriptional regulation of adipogenesis. Genes Dev. *14*, 1293-1307.

124. Rosenwald, M., Perdikari, A., Rülicke, T., Wolfrum, C. (2013). Bi-directional interconversion of brite and white adipocytes Nature Cell Biology *15*, 659-667.

125. Rothwell, N.J., and Stock, M.J. (1983). Luxuskonsumption, diet-induced thermogenesis and brown fat: the case in favour. Clinical Science *64*, 19–23.

126. Saito, M., Okamatsu-Ogura, Y., Matsushita, M., Watanabe, K., Yoneshiro, T., Nio-Kobayashi, J., Iwanaga, T., Miyagawa, M., Kameya, T., Nakada, K., Kawai, Y., Tsujisaki, M. (2009). High incidence of metabolically active brown adipose

tissue in healthy adult humans: effects of cold exposure and adiposity. Diabetes *58*, 1526–1531.

127. Salpeter, S.J., Klochendler, A., Weinberg-Corem, N., Porat, S., Granot, Z., Shapiro, A.M., Magnuson, M.A., Eden, A., Grimsby, J., Glaser, B., and Dor, Y. (2011). Glucose regulates cyclin D2 expression in quiescent and replicating pancreatic β-cells through glycolysis and calcium channels. Endocrinology. *7*, 2589-2598.

128. Sanchez-Gurmaches, J., and Guertin, D.A. (2014). Adipocytes arise from multiple lineages that are heterogeneously and dynamically distributed. Nat Commun. 5, 4099.

129. Samuvel, D.J., Sundararaj, K.P., Nareika, A., Lopes-Virella, M.F., and Huang, Y. (2009). Lactate boosts TLR4 signaling and NF-kappaB pathway-mediated gene transcription in macrophages via monocarboxylate transporters and MD-2 up-regulation. J Immunol. *182*, 2476–2484.

130. Sasaki, M., Knobbe, C.B., Munger, J.C., Lind, E.F., Brenner, D., Brüstle, A., Harris, I.S., Holmes, R., Wakeham, A., Haight, J., You-Ten, A., Li, W.Y. et al. (2012). IDH1(R132H) mutation increases murine haematopoietic progenitors and alters epigenetics. Nature. *488*, 656-659.

131. Schulz, T.J., Huang, T.L., Tran, T.T., Zhang, H., Townsend, K.L., Shadrach, J.L., Cerletti, M., McDougall, L.E., Giorgadze, N., Tchkonia, T., Schrier, D., Falb, D., Kirkland, J.L., Wagers, A.J., and Tseng, Y.H. (2011). Identification of inducible brown adipocyte progenitors residing in skeletal muscle and white fat. Proc Natl Acad Sci U S A *4*, 143-148.

132. Scimè, A., Grenier, G., Huh, M. S., Gillespie, M. a, Bevilacqua, L., Harper, M.-E., and Rudnicki, M. a (2005). Rb and p107 regulate preadipocyte differentiation into white versus brown fat through repression of PGC-1alpha. Cell Metabolism *2*, 283–295.

133. Scimè, A., Soleimani, V.D., Bentzinger, C.F., Gillespie, M.A., Le Grand, F., Grenier, G., Bevilacqua, L., Harper, M.E., and Rudnicki, M.A. (2010). Oxidative status of muscle is determined by p107 regulation of PGC-1alpha. J Cell Biol. *190*, 651–662.

134. Seale, P., Kajimura, S., Yang, W., Chin, S., Rohas, L.M., Uldry, M., Tavernier, G., Langin, D., and Spiegelman, B.M. (2007). Transcriptional control of brown fat determination by PRDM16. Cell Metabolism *6*, 38–54.

135. Seale, P., Bjork, B., Yang, W., Kajimura, S., Kuang, S., Scime, A., Devarakonda, S., Chin, S., Conroe, H.H.M., Erdjument-Bromage, H., Tempst, P., Rudnicki, M. A., Beier, D.R., Spiegelman, B.M. (2008). PRDM16 controls a brown fat/skeletal muscle switch. Nature *454*, 961–967.

136. Seale, P., Conroe, H.M., Estall, J., Kajimura, S., Frontini, A., Ishibashi, J., Cohen, P., Cinti, S., and Spiegelman, B.M. (2011). Prdm16 determines the thermogenic program of subcutaneous white adipose tissue in mice. The Journal of Clinical Investigation *121*, 53–56.

137. Sellayah, D., Bharaj, P., and Sikder, D. (2011). Orexin is required for brown adipose tissue development, differentiation, and function. Cell Metabolism *14*, 478–490.

138. Shepherd, P.R., Gnudi, L., Tozzo, E., Yang, H., Leach, F., and Kahn, B.B. (1993). Adipose cell hyperplasia and enhanced glucose disposal in transgenic mice overexpressing GLUT4 selectively in adipose tissue. J Biol Chem. *268*, 22243-22246.

139. Stanford, K.I., Middelbeek, R.J., Townsend, K.L., An, D., Nygaard, E.B., Hitchcox, K.M., Markan, K.R., Nakano, K., Hirshman, M.F., Tseng, Y.H., and Goodyear, L.J. (2013). Brown adipose tissue regulates glucose homeostasis and insulin sensitivity. J Clin Invest *123*, 215-223.

140. Suda, T., Takubo, K., and Semenza, G.L. (2011). Metabolic regulation of hematopoietic stem cells in the hypoxic niche. Cell Stem Cell. *9*, 298-310.

141. Su, X. and Abumrad, N.A. (2009). Cellular fatty acid uptake: a pathway under construction. Trends Endocrinol. Metab. *20*, 72-77.

142. Tang, Q.Q., and Lane, M.D. (2012). Adipogenesis: from stem cell to adipocyte. Annual Review of Biochemistry *81*, 715–736.

143. Tang, Q.Q., Otto, T.C., and Lane, M.D. (2003). Mitotic clonal expansion: a synchronous process required for adipogenesis. Proc Natl Acad Sci *100*, 44-49.

144. Tang, Q.Q., Otto, T.C., and Lane, M. D. (2004). Commitment of C3H10T1/2 pluripotent stem cells to the adipocyte lineage. Proceedings of the National Academy of Sciences of the United States of America *101*, 9607–9611.

145. Teperino, R., Amann, S., Bayer, M., McGee, S.L., Loipetzberger, A., Connor, T., Jaeger, C., Kammerer, B., Winter, L., Wiche, G. et al. (2012). Hedgehog partial agonism drives Warburg-like metabolism in muscle and brown fat. Cell. *151*,414-26.

146. Timchenko, N.A., Wilde, M., Iakova, P., Albrecht, J.H., and Darlington, G.J. (1999). E2F/p107 and E2F/p130 complexes are regulated by C/EBPalpha in 3T3-L1 adipocytes. Nucleic Acids Res. *27*, 3621–3630.

147. Timmons, J.A., Wennmalm, K., Larsson, O., Walden, T.B., Lassmann, T., Petrovic, N., Hamilton, D.L., Gimeno, R.E., Wahlestedt, C., Baar, K., Nedergaard, J., and Cannon, B. (2007). Myogenic gene expression signature establishes that brown and white adipocytes originate from distinct cell lineages. Proc Natl Acad Sci U S A *13*, 4401-4406.

148. Tormos, K.V., Anso, E., Hamanaka, R.B., Eisenhart, J., Joseph, J., Kalyanaraman, B., and Chandel, N.S. (2011). Mitochondrial complex III ROS regulate adipocyte differentiation. Cell Metab. *14*, 537–544.

149. Tseng, Y.H., Kokkotou, E., Schulz, T.J., Huang, T.L., Winnay, J.N., Taniguchi, C.M., Tran, T.T., Suzuki, R., Espinoza, D.O., Yamamoto, Y., Ahrens, M.J., Dudley, A.T., Norris, A.W., Kulkarni, R.N., Kahn, C.R. (2008). New role of bone morphogenetic protein 7 in brown adipogenesis and energy expenditure. Nature *454*, 1000–1004.

150. Valcourt, J.R., Lemons, J.M., Haley, E.M., Kojima, M., Demuren, O.O., and Coller, H.A. (2012). Staying alive: metabolic adaptations to quiescence. Cell Cycle. *11*, 1680-1696.

151. Vander Heiden, M.G., Cantley, L.C., Thompson C.B. (2009) Understanding the Warburg effect: the metabolic requirements of cell proliferation. Science *324*, 1029-1033.

152. van Marken Lichtenbelt, W.D., Vanhommerig, J.W., Smulders, N.M., Drossaerts, J.M., Kemerink, G.J., Bouvy, N.D., Schrauwen, P., and Teule, G.J. (2009). Cold-activated brown adipose tissue in healthy men. The New England Journal of Medicine *360*, 1500–1508.

153. Virtanen, K., Lidell, M., Orava, J., Heglind, M., Westergren, R., Niemi, T., Taittonen, M., Laine, J., Savisto, N.J., Enerback, S., and Nuutila, P. (2009). Functional Brown Adipose Tissue in Healthy Adults. New England Journal of Medicine *360*, 1518-1525.

154. Vanderluit, J.L., Wylie, C.A., McClellan, K.A., Ghanem, N., Fortin, A., Callaghan, S., MacLaurin, J.G., Park, D.S., Slack, R.S. (2007). The Retinoblastoma family member p107 regulates the rate of progenitor commitment to a neuronal fate. J Cell Biol. *178*, 129–139.

155. Vitali, A., Murano, I., Zingaretti, M.C., Frontini, A., Ricquier, D., and Cinti, S. (2012). The adipose organ of obesity-prone C57BL/6J mice is composed of mixed white and brown adipocytes. J Lipid Res. *53*, 619-629.

156. Wagner, G.R., and Payne, R.M. (2011). Mitochondrial acetylation and diseases of aging. J Aging Res. *2011,* 234875.

157. Waldén, T.B., Hansen, I.R., Timmons, J.A., Cannon, B., and Nedergaard, J. (2012). Recruited vs. nonrecruited molecular signatures of brown, "brite," and white adipose tissues. Am J Physiol Endocrinol Metab *1*, E19-31.

158. Wallace, D.C., and Fan, W. (2010). Energetics, epigenetics, mitochondrial genetics. Mitochondrion. 10,12-31.

159. Wang, Q.A., Tao, C., Gupta, R.K., and Scherer, P.E. (2013) Tracking adipogenesis during white adipose tissue development, expansion and regeneration. Nat Med. *19*, 1338–1344.

160. Ward, P.S., and Thompson, C.B. (2012). Metabolic reprogramming: a cancer hallmark even warburg did not anticipate. Cancer Cell *21,* 297–308.

161. Wellen, K.E., Hatzivassiliou, G., Sachdeva, U.M., Bui, T.V., Cross, J.R., Thompson, C.B. (2009). ATP-citrate lyase links cellular metabolism to histone acetylation. Science. 324, 1076-1080.

162. Wellen, K.E., and Thompson, C.B. (2012). A two-way street: reciprocal regulation of metabolism and signalling. Nat Rev Mol Cell Biol. *13,* 270–276.

163. Wirt, S.E., and Sage, J. (2010). p107 in the public eye: an Rb understudy and more. Cell Division *5*, 9.

164. Wu, J., Boström, P., Sparks, L.M., Ye, L., Choi, J.H., Giang, A.H., Khandekar, M., Virtanen, K. a, Nuutila, P., Schaart, G., Huang, K., Tu, H., van Marken Lichtenbelt, W.D., Hoeks, J., Enerbäck, S., Schrauwen, P., Spiegelman, B.M. (2012). Beige adipocytes are a distinct type of thermogenic fat cell in mouse and human. Cell *150*, 366–376.

165. Wu, M.V., Bikopoulos, G., Hung, S., and Ceddia, R.B. (2014). Thermogenic capacity is antagonistically regulated in classical brown and white subcutaneous fat depots by high fat diet and endurance training in rats: impact on whole-body energy expenditure. J Biol Chem. 289, 34129-34140.

166. Yu, Z.K., Wright, J.T., and Hausman, G.J. (1997). Preadipocyte recruitment in stromal vascular cultures after depletion of committed preadipocytes by immunocytotoxicity. Obes Res *5*, 9-15.

167. Xu, W., Yang, H., Liu, Y., Yang, Y., Wang, P., Kim, S.H., Ito, S., Yang, C., Xiao, M.T., Liu, L.X. et al. (2011). Oncometabolite 2-hydroxyglutarate is a competitive inhibitor of alpha-ketoglutarate-dependent dioxygenases. Cancer Cell. *19*, 17-30.

168. Xue, B., Rim, J.S., Hogan, J.C., Coulter, A.A, Koza, R.A, and Kozak, L.P. (2007). Genetic variability affects the development of brown adipocytes in white fat but not in interscapular brown fat. Journal of Lipid Research *48*, 41–51.

169. Yanes, O., Clark, J., Wong, D.M., Patti, G.J., Sánchez-Ruiz A, Benton, H.P., Trauger, S.A., Desponts, C., Ding, S. and Siuzdak, G. (2011). Metabolic oxidation regulates embryonic stem cell differentiation. Nat Chem Biol. *6*, 202-204

170. Young, A.P., Nagarajan, R., Longmore, G.D. (2003). Mechanisms of transcriptional regulation by Rb-E2F segregate by biological pathway. Oncogene *22*, 7209-7217.

171. Zaidi, N., Swinnen, J. V, and Smans, K. (2012). ATP-citrate lyase: a key player in cancer metabolism. Cancer Research *72*, 3709–3714.

172. Zavitz, K. H., and Zipursky, S. L. (1997). Controlling cell proliferation in differentiating tissues: genetic analysis of negative regulators of Gl- S-phase progression. Current Opinion in Cell Biology *9*, 773–781.

173. Zhang, Y.M., Marsboom, G., Toth, P.T., and Rehman, J. (2013). Mitochondrial respiration regulates adipogenic differentiation of human mesenchymal stem cells. PLoS One. *8*, e77077.

174. Zhou, W., Choi, M., Margineantu, D., Margaretha, L., Hesson, J., Cavanaugh, C., Blau, C.A., Horwitz, M.S., Hockenbery, D., Ware, C., and Ruohola-Baker, H. (2012). HIF1α induced switch from bivalent to exclusively glycolytic metabolism during ESC-to-EpiSC/hESC transition. EMBO J. *31*, 2103-2116.

175. Zhu, L., van den Heuvel, S., Helin, K., Fattaey, A., Ewen, M., Livingston, D., Dyson, N., and Harlow, E. (1993). Inhibition of cell proliferation by p107, a relative of the retinoblastoma protein. Genes & Development *7*, 1111–1125.

176. Zini, N., Trimarchi, C., Claudio, P. P., Stiegler, P., Marinelli, F., Maltarello, M. C., La ala, D., De Falco, G., Russo, G., Ammirati, G., Maraldi, N. M., Giordano, A. and Cinti, C. (2001). pRb2/p130 and p107 control cell growth by multiple strategies and in association with different compartments within the nucleus. Journal of Cellular Physiology *189*, 34–44.